Journal of Energy Storage 160 (2026) 121580

Contents lists available at ScienceDirect

Journal of Energy Storage

journal homepage: www.elsevier.com/locate/est

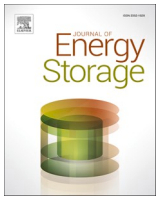

Research Papers

Enhancing the interoperability of smart grids with active and proactive strategies in the presence of energy storage units

Diogo Filipe Azevedo Souto Ramos [a], Mohammad Sadegh Javadi [b,*]

[a] Faculty of Engineering, University of Porto, 4200-465, Porto, Portugal
[b] Research Center for Systems and Technologies (SYSTEC), Advanced Production and Intelligent Systems Associate Laboratory (ARISE), Faculty of Engineering, University of Porto, 4200-465, Porto, Portugal

ARTICLE INFO

Keywords:
Energy storage system
High-impact-low-probability events
Monte-Carlo simulation
Multi-temporal optimal power flow
Network reconfiguration
Smart grids

ABSTRACT

Transitioning from a centralized power system infrastructure to a decentralized power system with power generation spread across the distribution network is a rather new shift in modern society. This transition has introduced challenges in achieving resilience and interoperability on the distribution network as well as new technological demands from its users. This study addresses these challenges by focusing primarily on low-voltage and medium-voltage distribution networks, due to their limited redundancy and radial structure, which introduces susceptibility to energy disruptions. Such disruptions can be caused by several factors, often introducing complex situations. Generally, they can be grouped into two sections: man-made and nature-related, with their probability of occurrence being low. These vulnerabilities on the distribution network are expanded while the integration of renewable energy and systems to store energy is increasing. The main motivation for this research arises from the increasing need for reliable, modular, and sustainable systems capable of withstanding normal and extreme conditions. In these extreme conditions, high-impact, low-probability events play a major part as they range from natural disasters to man-made disruptions. While there are solutions, they often fall short of ensuring seamless interoperability between diverse components. To address these issues, this study proposes the development of a multi-temporal, modular, and scalable framework built on the principles of integrated digitalized energy systems, which includes scenario-based simulations on the modified IEEE 33-bus and IEEE 69-bus distribution networks. The core objective is to minimize energy not supplied given a load's priority across a time interval, especially during disruptive scenarios. The quantitative results demonstrate that the proposed strategies reduced energy not supplied from 57.8 MWh to 57.6 MWh in the modified IEEE 33-bus system and significantly from 33.1 MWh to 31.5 MWh in the modified IEEE 69-bus system under worst-case scenarios. With the integration of energy storage systems, the average Resilience Index improved to 32% compared to 30% without the inclusion, for the modified IEEE 33-bus network, and 58% for the modified IEEE 69-bus network with the inclusion of energy storage systems compared to 55% without the inclusion. The findings indicate that storage deployment offers greater resilience benefits in the modified IEEE 69-bus network compared to smaller ones. Ultimately, this study contributes to the development of smart distribution systems capable of maintaining functionality under stress, while aligning with key United Nations Sustainable Development Goals for affordable, reliable, and sustainable energy infrastructure.

1. Introduction

Today's society is completely different from the 20th century society. The current era is evolving at a rapid pace, where each community needs more energy for a faster moment's notice. Since then, the electrical power system has become the pillar of global industrial development and even the backbone of everyday life [1]. With the passing of years, renewable energy gained a lot of attraction because of its fast evolution and competitiveness and became an indispensable energy source. This attraction was in the form of integration of distributed energy sources (DERs), such as photovoltaic (PV), wind power (WP), and electric vehicles (EVs) [2]. Not only that, but as the communities' demand for more sustainable, reliable, and autonomous electricity networks increases, achieving interoperability across interconnected systems becomes essential, especially within medium-voltage (MV) and low-voltage (LV)

* Corresponding author.
E-mail address: Javadi@fe.up.pt (M.S. Javadi).

https://doi.org/10.1016/j.est.2026.121580
Received 5 October 2025; Received in revised form 22 February 2026; Accepted 13 March 2026
Available online 1 April 2026

Nomenclature

Indices

d	Index for DR blocks
i,j	Index for nodes
l	Index of lines
g	Index of generators
k	Index of storage systems
t	Index for time

Sets

Λ	Set of nodes with DR programs
EMG	Set of load nodes in MGs with extra power
M	Set of nodes with distributed generations
L	Set of nodes with loads

Parameters

Φ_i	Power factor
$\eta_k^{Chr}, \eta_k^{Dchr}$	Charging/discharging efficiency
Δt	Time interval (1 h)
$P_{i,t}^{LD}$	Active load at node i in per unit
$P_i^{G,min}$	Active power lower limit for DG at bus i
$P_i^{G,max}$	Active power upper limit for DG at bus i
$P_{id,t}^{DR,b}$	Capacity of DR block d of load i
E_k^0	Initial energy stored in the EES
$S_{i,t}^{G,Max}$	Max apparent power of DG at node i
$P_{ij,t}^{Max}$	Maximum active power through line ij
$P_{k,max}^{Chr}$	Maximum charging power of the battery
$P_{k,max}^{Dchr}$	Maximum discharging power of the battery
$Q_{ij,t}^{Max}$	Maximum reactive power through line ij
E_k^{min}, E_k^{max}	Minimum/Maximum stored energy in the battery
$Pr_{id,t}^{DR}$	Priority factor of DR block d of the load i
$Pr_{i,t}^{L}$	Priority factor of the load at node i
X_{ij}	Reactance of the line from node i to node j
$Q_{ij,t}^{G,Min}$	Reactive power lower limit for DG at node i
$Q_{ij,t}^{G,Max}$	Reactive power upper limit for DG at node i
R_{ij}	Resistance of the line from node i to node j
$I_{ij}^{2,Max}$	Squared current capacity limit of the line ij
$V_{i,t}^{Min}$	Voltage magnitude lower limit at node i
$V_{i,t}^{Max}$	Voltage magnitude upper limit at node i

Continuous variables

$\theta_{i,t}$	Phase angle of bus i
$\sigma_{i,t}$	Supply disruption at node i
$\delta_{id,t}^{DR}$	Used portion of DR block d of the load i in CLR
$\varphi_{d,t}^{DR}$	Linearized curtailed power from DR block d at time t
$P_{i,t}^{L}$, $Q_{i,t}^{L}$	Active/Reactive power load at node i
$P_{k,t}^{Chr}$	Charged Power on EES k
$P_{i,t}^{LC}$	Curtailed load at node i
$P_{k,t}^{Dchr}$	Discharged Power on EES k
$P_{ij,t}^{l}, Q_{ij,t}^{l}$	Hourly Active/Reactive Power through line ij
$P_{ji,t}$	Hourly active power transmitted from node j to node i
$P_{ij,t}^{Loss}, Q_{ij,t}^{Loss}$	Hourly active/reactive power loss of line *ij*
$Q_{ji,t}$	Hourly reactive power transmitted from node j to node i
$P_{i,t}^{inj}$	Net hourly active power injection at node i
$Q_{i,t}^{inj}$	Net hourly reactive power injection at node i
$P_{i,t}^{DR}$	Power reduced by DR program at node i
$I_{ij,t}^{2}$	Squared current magnitude through line ij
$V_{ij,t}^{2}$	Squared voltage magnitude through line ij
$P_{i,t}^{LS}$	Restored active load at node i
$Q_{i,t}^{LS}$	Restored reactive load at node i

Binary variables

ν_{ij}	Binary variable: Directional connectivity link from node *i* to node *j*
$\omega_{id,t}^{LS}$	Binary variable: If the DR block *d* of load *i* is used = 1, if not = 0
$I_{k,t}^{Ch.}$, $I_{k,t}^{Dch.}$	Binary variable: If the EES is charging = 1, if the EES is not charging =0
$z_{k,t}$	Binary variable: If the EES discharging stopped = 1, if not = 0
$y_{ij,t}$	Binary variable: If the line *ij* is closed = 1, if the line is closed = 0
$\omega_{i,t}^{LS}$	Binary variable: If there's curtailment of the load = 1, if it's partially or fully restored = 0
$LS_{i,p,t}$	Load curtailment status

Abbreviations

AI	Artificial Intelligence
AMI	Advanced metering infrastructure
DERs	Distributed energy sources
DFR	Dynamic feeder reconfiguration
DR	Demand Response
DSO	Distribution System Operator
EES	Electrical Energy Storage
ENS	Energy Not Supplied
EVs	Electric vehicles
GA	Genetic Algorithms
GAMS	General Algebraic Modelling System
GBD	Generalized Benders Decomposition
GES	Grid-scale energy storage
HILP	High-impact low-probability
HSS	Hydrogen Storage Systems
HV	High Voltage
IDES	Integrated Digitalized Energy System
KVL	Kirchhoff's Voltage Law
LECs	Local energy communities
LV	Low Voltage
MIQCP	Mixed Integer Quadratically Constrained Program
MISOCP	Mixed Integer Second Order Cone Programming
ML	Machine learning
MTOPF	Multi-Temporal Optimal Power Flow
MV	Medium Voltage
NMGs	Networked microgrids
PLL	Phase Lock Loop
PMUs	Phasor measurement units
PV	Photovoltaic
RES	Renewable Energy Sources
RI	Resilience Index
SoC	State of Charge
SOCP	Second-Order Cone Programming
WP	Wind Power

networks [3]. With the introduction of renewable energy, it became easy, accessible, and affordable for end-users to produce small amounts of energy in local energy communities (LECs), leading to the system being distributed [4]. Not only that, this introduction allowed the power flow to be bidirectional, letting consumers not only consume energy from the grid but also produce and sell it back to the grid, transitioning the traditional distribution networks towards active power grids.

Another topic to focus on is the involvement of the Integrated Digitalized Energy System (IDES). IDEs are an ecosystem that leverages end-user engagement, distributed energy resources, and flexible grid-following and grid-forming technologies to optimize energy generation, distribution, and consumption. Not only that, but they facilitate real-time data exchange, enabling seamless energy flows. A smart grid is defined as an intelligent and controlled electrical grid with the ability to distribute electricity from its generation to end consumers while communicating and delivering information to analyze the behavior of both suppliers and consumers.

1.1. Motivation

Modern technology advancements allow the modern electrical grid to shape the future of electrical grids; however, they face growing demands for reliability and flexibility as they move away from centralized systems. The decentralized system adds resilience and sustainability but also requires a high level of interoperability to coordinate resources and energy flows, making monitoring the grid a hard task [5]. Additionally, smart grids integrate various energy storage units that introduce new challenges and opportunities in ensuring grid reliability, resilience, and flexibility [6]. Traditional centralized energy systems are increasingly challenged by recurring disruptions, such as weather, cyber-attacks, and the old age of the current infrastructure. Real-world energy systems face rising energy demands; the IDEs offer a new approach to integrating these resources. With the implementation of real-time interoperability, IDEs bolster resilience by preparing networks to withstand and recover from disruptions [7]. The flexibility and decentralized control mechanisms ensure that critical loads, such as hospitals and schools, are met even during grid outages, minimizing service interruptions and customer impacts. Not only that but giving priority to such institutions that need to be carefully maintained for the better good of society has the highest priority. With that said, this research aims to improve the grid's resilience and its flexible power systems that can sustain operations through high-impact low-probability (HILP) events.

1.2. Literature review

Resilience in energy systems refers to the ability to withstand and rapidly recover from disruptions, whether they are natural disasters, cyber-attacks, or equipment failures due to external or internal influences [8]. A resilient energy system must withstand shocks by absorbing the impact of disturbances without significant service interruptions while recovering quickly to restore critical services first. While a resilient system must withstand shocks, it should be able to adapt and learn from past events and continuously improve its shock-withstanding ability [9]. Resilience strategies are essential for ensuring reliable power delivery. However, these systems face growing challenges due to the increasing frequency of natural disasters, human-induced risks, and the integration of renewable energy sources (RES). To overcome this, three main resilience strategies are used: system hardening, operational optimization, and DER-based restoration [10].

Traditional power system assessment has primarily focused on reliability analysis, which evaluates system performance under low-impact high-probability (LIHP) events, such as routine component failures, equipment aging, or short-duration outages caused by localized faults. While the reliability indices provide valuable insights into average service continuity, they inherently emphasize frequent and statistically independent disturbances, often overlooking rare but catastrophic events that can result in widespread and prolonged outages [11].

In contrast, HILP events, such as hurricanes, extreme windstorms, floods, earthquakes, wildfires, and coordinated cyber-physical attacks, pose fundamentally different challenges to power systems [12]. Although these events occur infrequently, their consequences can be severe, leading to extensive infrastructure damage, long restoration times, and significant socio-economic impacts [13]. Recent studies have shown that extreme weather events account for a growing share of major power outages worldwide, a trend further exacerbated by climate change and increasing climate variability [14]. These developments highlight the limitations of reliability-centered planning frameworks when applied to extreme and large-scale disruptions.

The cascading and interdependent nature of HILP failures necessitates assessment approaches that explicitly capture system degradation, recovery trajectories, and adaptive responses over time. Consequently, resilience assessment places greater emphasis on attributes such as robustness, resourcefulness, rapidity, and adaptability, rather than solely on failure frequency or expected outage duration [15]. This paradigm shift underscores the importance of resilience-oriented metrics and modelling frameworks that can adequately represent system behavior under extreme but plausible HILP scenarios.

Operational optimization is the improvement of the efficiency and effectiveness of grid operations to enhance resilience. Utilizing real-time data collection from smart meters and sensors, this data-driven approach allows for dynamic adjustments to power flows and load management, ensuring that critical loads are prioritized during disruptions [16]. Additionally, the Multi-Temporal Optimal Power Flow (MTOPF) model can help in planning and operating microgrids under both normal and extreme conditions, thereby improving resilience [17]. While the conventional optimal power flow models are effective for instantaneous dispatch, they treat every hour as an isolated snapshot. This approach is insufficient for resilient microgrids because it ignores time-coupling constraints, particularly the inter-temporal state of EES and load restoration continuity [18]. The MTOPF model adopted here bridges this gap by simultaneously optimizing a 24-h horizon, ensuring that decisions made for energy storage charging or load variations are viable for ongoing time steps [19].

Alternative methods offer different trade-offs for distribution resilience. AI and Data-Driven approaches, allow for fast reconfiguration. However, these methods often function as ‘black boxes’ that cannot rigorously guarantee safety constraints during critical HILP events compared to physical models [20]. While robust, they often suffer from excessive computational burdens that scale poorly with network size. By utilizing a scenario-based MTOPF approach like rolling-horizon strategies, this work preserves the rigorous safety guarantees of optimization while remaining computationally tractable for operational planning.

If, for some reason, the grid must be operated under extreme conditions, the operator must have control over the adjustments of consumers' energy usage during peak hours or emergencies [21]. Not only that, but Dynamic Feeder Reconfiguration (DFR) allows the grid to isolate faults and reroute power dynamically, reducing the Energy-Not-Served (ENS) during emergencies [22].

Active and proactive strategies play distinct yet complementary roles that together contribute to a more resilient and efficient energy network. Active strategies are characterized by their focus on real-time interaction with grid components and on dynamic response to events as they unfold [21]. These mechanisms typically rely on adaptive communication protocols and on distributed agents that negotiate power flows. The strength of active approaches lies in their capacity to adapt swiftly to unforeseen disturbances, ensuring that localized control loops can maintain stability even when measurements or conditions deviate sharply from expectations [23].

Proactive strategies, by contrast, emphasize anticipation and preparation. They leverage historical data, forecasting algorithms, and model-based simulations to identify potential challenges before they occur, allowing the system to reconfigure itself in advance or deploy

contingency plans during planned maintenance windows [24]. Similarly, predictive analytics may forecast load patterns or fault probabilities days in advance, enabling the scheduling of energy storage charging and discharging so that resources are positioned optimally when they are most needed. Although proactive measures can greatly reduce the likelihood and severity of foreseeable issues, they depend heavily on the accuracy of forecasting models and on extensive computational resources for simulation and planning [25].

HILP events, as the name suggests, are events with high societal impact that happen occasionally but are regarded as having a low stochastic probability of occurring. However, when these events occur, a wide area interruption can follow, and the electricity supply is not assured. This interruption in the supply of critical loads provokes a severe impact on society's critical functions [26]. Natural disasters, such as hurricanes, earthquakes, and wildfires, fall into the category of HILP events as they pose significant risks to the stability of society's function, but are rare or have a low probability of occurring. Not only that, but cyber-attacks also fall in the HILP category. As our grid is modernizing and implementing digital technologies, cyber-attacks are prone to happen [27]. As grids become more interconnected and composed of digital technologies, they become more vulnerable to these types of attacks. So, to address these attacks and challenges, it's important to have resilience strategies that can withstand both natural and human-induced disruptions. This includes investing in advanced monitoring technologies and enhancing grid flexibility [28].

The study in [29] addresses the resilient operation of smart distribution grids under physical-cyber-attacks, focusing on HILP events. The authors classify such events into natural hazards and human-induced attacks, emphasizing the latter due to the increasing vulnerabilities in smart grids. The study proposes a comprehensive framework to enhance grid resilience by integrating RES and EES, leveraging robust optimization to model worst-case scenarios under cyber-physical threats.

The study introduces a resiliency index based on load interruption metrics, evaluating system performance under Denial-of-Service (DoS) and False Data Injection (FDI) attacks. Simulations on modified IEEE 33-bus and real 43-bus systems demonstrate that RES and EES significantly improve resilience, with the resiliency index remaining high even under severe conditions. The work also highlights the critical role of DERs in mitigating disruptions and ensuring sustainable energy supply, while also identifying gaps for future research, such as advanced robust optimization techniques and economic considerations in resilient grid operation [30]. However, while this framework effectively addresses robustness against malicious attacks, it simplifies the physical constraints of the grid by not accounting for the unbalanced nature of residential LV networks or the potential of granular demand-side flexibility to proactively mitigate the impact of natural hazards.

Recent advancements in energy storage scheduling and grid resilience have highlighted the critical role of DERs and EESs in mitigating the impacts of HILP events. The Authors in [31] address the challenge of balancing economic efficiency with disaster preparedness by proposing a variable-type minimum State of Charge (SoC) strategy for EESs and hydrogen storage systems (HSSs). Their research demonstrates that while traditional fixed-type SOC methods prioritize economic gains, they often fail to ensure sufficient energy reserves during outages. In contrast, the variable-type SOC approach dynamically adjusts storage reserves based on anticipated demand, improving power supply capacity by 11.43% to 18.53% despite a modest 2.5% to 2.8% increase in operational costs while incorporating Monte-Carlo simulations to model stochastic disaster scenarios. Despite these improvements in storage management, the strategy in [31] remains isolated from broader active network management techniques, lacking integration with dynamic topology reconfiguration or the coordination of grid-forming units which are essential for maintaining stability in islanded LV networks.

Related to microgrid management, the Authors in [32] proposed an MTOPF model designed for both normal and contingent operations due to the likes of HILP events. The optimization model is formulated as a mixed-integer quadratically constrained programming (MIQCP) problem, with a Second-Order Conic Programming (SOCP) to efficiently manage the quadratic constraints inherent in power flow equations. The objective function attempts to minimize total operational costs, comprising the cost of energy from dispatchable generators and the main grid, the utilization cost of the Electrical Energy Storage (EES), while modelling the dynamic behavior of their systems over the planning horizon, and to prevent load curtailment during normal operation. This model was implemented on a modified IEEE 33-bus test system, which comprised two DERs (one photovoltaic and one wind generator) and two thermal generators. The loads were categorized with a priority index related to how important they were to remain supplied in times of contingent operation. In such an islanded operation scenario, the model successfully reconfigures the network and coordinates local resources, showing how the coordination of DERs allows the supply of priority loads. A significant limitation of this model, however, is its reliance on balanced network assumptions, which fails to capture the realistic phase-unbalanced characteristics of LV distribution networks where residential loads and single-phase renewables are connected.

In [33], the formation of Networked microgrids (NMGs) is explored as a strategy to enhance operational flexibility and resilience in distribution networks, particularly during extreme weather events and large-scale emergencies, more precisely HILP events. The proposed methodology incorporates dynamic network reconfiguration while incorporating DERs, more particularly, PV systems, and EES. A multi-temporal 24 h horizon approach, on the modified IEEE 33-bus system, quantified power imbalances that may occur in each MG and tracked DER operational status, such as SoC. This approach allowed a reduction in load shedding (LS) by 33.5% in standalone configurations and up to 57.5% when there were power exchanges between micro-grids (MGs). While effective at the medium-voltage level, this methodology does not fully explore the 'bottom-up' flexibility available from residential end-users, largely overlooking the potential of smart metering infrastructure to unlock responsive flexibility at the household level.

In [34], it's introduced an automated and rapid load restoration strategy centered on optimal DFR is introduced. The research proposes a centralized EMS that can reconfigure a microgrid's topology to supply high-priority loads at minimal cost during both grid-connected and islanded-mode operations. The model forms intentional, autonomous microgrids, each requiring a grid-forming unit. The methodology is formulated as an MIQCP that integrates an OPF problem. The model's efficacy was demonstrated on a modified IEEE 33-bus system with multiple DGs, two of which possess grid-forming capabilities. In a simulated HILP event that serves the utility connection, the EMS successfully formed two independent microgrids by executing optimal switching actions. The results show that the system restored all critical loads, a considerable portion of medium-priority loads, and some low-priority loads, all while respecting DG capacity limits and converging to a solution in just 13 s. This demonstrates the model as a fast and accurate tool for real-world resilience enhancement. Nevertheless, similar to previous studies, this strategy focuses heavily on reactive measures like switching actions and generation dispatch, neglecting the unified modelling of preventive and restorative time horizons and failing to adequately address how proactive demand-side management can complement grid-forming units.

In [35], a bi-level framework is proposed to enhance the resilience of integrated electricity-gas-heating networks by leveraging energy hubs, fast-acting flexible loads, electric vehicles (EVs), power-to-gas (P2G) technologies, and gas storage systems. However, for this current study, only the fast-acting flexible loads portion of the work done is relevant. The study addresses uncertainties in load, RES, and DR participation using a scenario-based method. The case studies used demonstrate that DFR increases the resilience index by 36.32% during line outages. The framework highlights the synergistic benefits of multi-energy coordination, dynamic topology adjustments, and distributed resource integration for resilient operation under extreme events equivalated to HILP

Table 1
Comparison of features in literature review.

Reference	LV	MTOPF	EES	RES	DFR	Network Restoration	HILP	Priority	RI	DR	Multiple Case Studies
[29]	✗	✗	✓	✓	✗	✗	✓	✗	✓	✗	✗
[31]	✗	✗	✓	✓	✗	✗	✓	✓	✓	✗	✗
[32]	✗	✓	✓	✓	✓	✓	✓	✓	✗	✗	✗
[33]	✗	✓	✓	✓	✓	✓	✗	✗	✗	✗	✗
[34]	✓	✗	✓	✓	✓	✓	✓	✓	✓	✗	✗
[35]	✓	✗	✓	✓	✓	✗	✗	✓	✗	✗	✗
[36]	✓	✗	✗	✓	✓	✓	✓	✓	✗	✓	✓
[37]	✓	✓	✓	✓	✓	✓	✓	✓	✓	✓	✗
This Work	✓	✓	✓	✓	✓	✓	✓	✓	✓	✓	✓

events. The study in [36] presents a two-stage methodology to enhance network resilience during HILP events by MGs, DGs, and DR programs for Critical Load Restoration (CLR). The novelty of this work lies in its integrated consideration of MG ownership and incentive-based DR contracts to optimize the reconfiguration and resource allocation during post-disaster service restoration. In the first stage, a heuristic is used to determine post-event electrical islands and their radial reconfiguration, prioritizing minimal electrical distances between critical loads and DGs. The second stage applies a generalized Benders Decomposition (GBD) to solve a Mixed-Integer Second-Order Cone Programming (MISOCP) model. The objective is to maximize the restored critical loads while factoring in DR participation and operational constraints. The model distinguishes between privately owned and publicly owned MGs. Only MGs with DR contracts may allow curtailment of their loads in exchange for incentives, thereby enabling surplus power to be redirected elsewhere. The DR contracts are modeled as multi-block emergency DR programs with increasing priorities/prices.

While [35] and [36] offer robust market-based and multi-energy solutions, they tend to abstract the physical complexities of the electrical distribution grid, specifically not accounting for the technical constraints of three-phase unbalanced flows in LV networks.

Lastly, the work done by [37] introduces a comprehensive and scalable framework for resilience enhancement within LECs. The study proposes an MTOPF model that accounts for three-phase unbalanced LV networks and integrates diverse DERs, including Grid-scale energy storage (GES), photovoltaics, and demand-side flexibility. The work shows a unified modelling of network operations across preventive, corrective, and restorative time horizons, enabling a dynamic and proactive approach to HILP resilience planning. The model includes the ability for grid-forming GES units to operate in both grid-connected and islanded modes, thereby supporting intentional microgrid islanding in emergency scenarios. To evaluate resilience performance, the study develops a time-dependent RI that quantifies ENS relative to a baseline, while accounting for multi-priority customer loads, demand restoration profiles, and flexible contracted power levels. The framework is stress-tested using a five-layer HILP event simulator, which combines spatial-temporal fragility curves, sequential Monte-Carlo simulation, and windstorm trajectory modelling to generate realistic outage scenarios across MV and LV electrical grids. By utilizing energy system planning, operational control, and resilience engineering, this work contributes a robust methodological foundation and decision-support tool that guides distribution system operators in both real-time operations and long-term infrastructure planning under uncertainty.

Addressing these identified research gaps, namely, the lack of unbalanced network modelling, the separation of proactive and reactive strategies, and the limited integration of granular demand-side flexibility, this work aims to provide a holistic solution. Table 1 provides a summary comparing previous studies with the proposed dissertation work, based on the survey conducted of the primary focus of each work. As a result, this proposed dissertation is the result of all the previous key points.

1.3. Novelties and contributions

This paper focuses on enhancing the network resilience index in the occurrence of natural hazards, mainly windstorms. In order to leverage the interoperability of the smart distribution networks, both active and proactive actions have been captured in the developed optimization model. The active actions include optimal operation of DERs, optimal rescheduling of dispatchable DGs, strategic management of energy storage units, as well as optimal network reconfiguration throughout optimal switching actions. Proactive actions investigate the prioritization of loads and categorize them into high, medium, and low priority loads, as well as the DR contracts that allow the DSO to optimally manage the resources during HILP events. The main contributions of this study are threefold:

- Active and proactive strategies for resiliency enhancement.
- Optimal management of resources in normal and contingent events.
- Activating the demand response blocks in emergencies.

To facilitate the optimal operational planning of the distribution networks under HILP events, an advanced and fast MTOPF model has been developed in this study, and the proposed model has been implemented into an MIQCP optimization problem that can be solved using CPLEX solver. The optimal formation of the islanded microgrids, considering at least one grid-forming unit to serve the frequency and voltage reference, has been implemented and demonstrated using proper simulation results.

1.4. Paper organization

This paper is organized into four main sections: Section 2 provides the methodology for network assessment and resiliency analysis of distribution networks under windstorms. Section 3 addresses the mathematical problem formulations developed for both normal and contingent events. The simulation results on modified IEEE 33-bus networks are presented in Section 4 and demonstrating several case studies and scenarios for validation and application of the developed methodology. The concluding remarks of this paper are presented in Section 5.

2. Methodology assessment

This chapter outlines the methodology assessment of the work's inner workarounds. This assessment is particularly focused on the probability of failure of towers and lines based on the Monte-Carlo Simulation with Bernoulli's trials. Furthermore, it is concluded what HILP event this

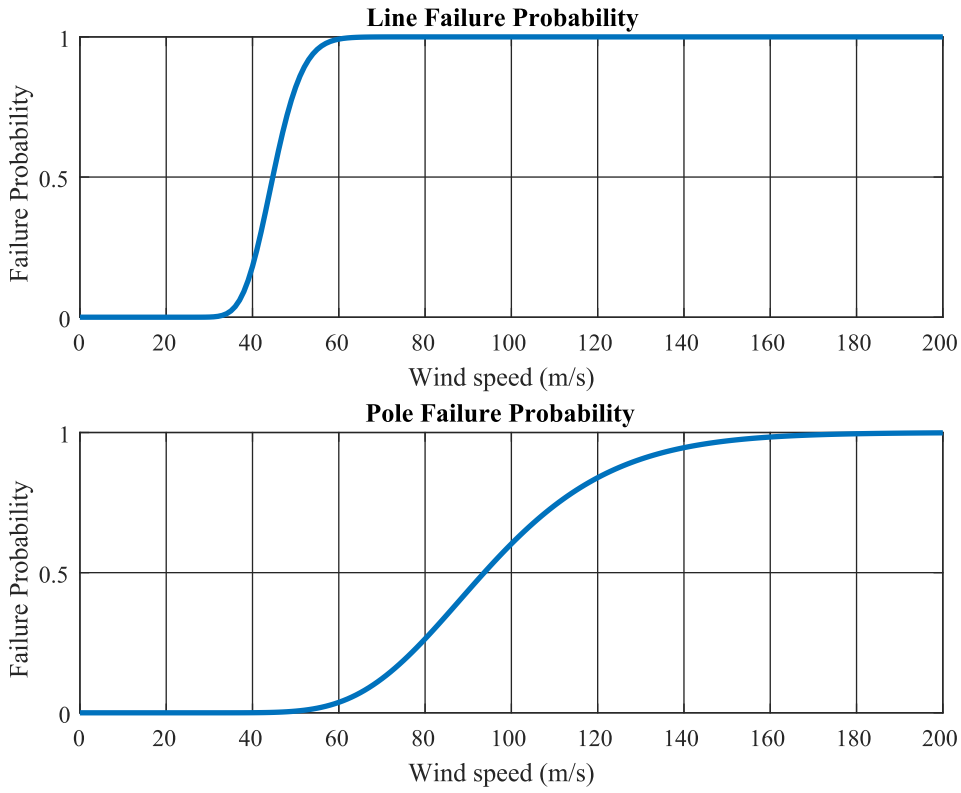

Fig. 1. Lines and poles failure probability distribution functions [38].

work will focus on and how it was achieved.

Analyzing the stability of the electrical grid under different scenarios is not only done through highly burden calculations, but also through an assessment of the resilience framework. Improving the redundancy of the network and hardening the system, considering the investment cost and time, is a valuable partial solution to the problem of stability, but it lacks consideration of the grid's physical components. The physical components that are worth talking about are the towers and lines that make up the electrical grid.

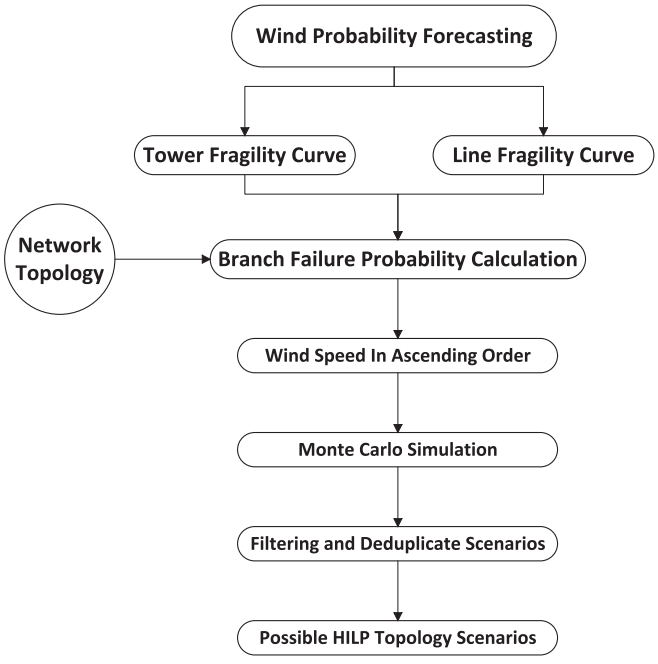

Fig. 2. Implementation of Monte-Carlo simulation for HILP generation scenarios.

2.1. Fragility assessment of distribution network assets

Modern electrical networks consist of several kilometers of power lines and hundreds or thousands of towers, and if a single tower along a line fails, a cascade effect may occur, potentially taking the entire branch out of service. With this, it is important to assess the fragility of the towers and lines when they are exposed to HILP events where abnormal conditions are commonplace. Typically, to assess the fragility of a network, historical failure data is required to plot a graph considering the relationship between hazard intensity and the probability of failure. In this study, the hazard is windstorm, and to approximate the probability of failure of distribution network assets, including feeders and poles, a specific probability distribution function has been incorporated [38]. This approach allows for modelling HILP events, where the tail of the distribution captures rare but severe occurrences. The resulting fragility curve provides a theoretical estimation of how the system's components respond to escalating windstorm speeds. The cumulative probability of line and tower failures can be seen in Fig. 1.

It should be noted that these fragility curves refer to the independent collapse of a single pole and distribution lines. The mathematical representation of the line outage probability distribution function is as follows:

$$P_{br} = P_{br,B} + P_{br,T} - P_{br,B}P_{br,T} \quad (1)$$

In Eq. (1), P_{br} represents the probability of a line failure as a function of wind speed, while $P_{br,B}$ and $P_{br,T}$ denote the probabilities of failure due to conductor failure and tower collapse, respectively. The probability,$P_{br,B}$, is obtained from the fragility curve shown in Fig. 1. It is assumed that the distribution poles fail independently, and each has the same probability of failure, $P_{br,T}$, as given in Eq. (2):

$$P_{br,T}(w) = 1 - \left(1 - P_{T,ind}(w)\right)^{N_T} \quad (2)$$

In Eq. (2), $P_{T,ind}(w)$ is the individual pole failure probability, and N_T is the number of poles along the feeder.

In this regard, the P_{br} is defined to identify which branches are vulnerable to windstorms. If P_{br} exceeds a specified threshold, the line is considered vulnerable, and the probability of each element will be considered in the generation of possible failure scenarios using Monte-Carlo Simulations [39].

2.2. Scenario generation using Monte-Carlo simulations

Regarding the numerous existing HILP events, high wind speeds have been chosen to evaluate the potential impact of failures on the electrical grid via a Monte-Carlo simulation. This simulation allows the system operators to model uncertainty by generating a large number of scenarios where it is possible to observe the resulting network behavior under those conditions.

For each scenario, a wind speed value is sampled from a lognormal distribution and used as an input to the pole and line failure probability models. Given a sampled wind speed, the corresponding failure probabilities for overhead lines and poles are calculated exclusively using the outage probability equations introduced in the previous section and the associated fragility curves shown in Fig. 2. These equations express the probability of outage as a logarithmic function of wind speed, and no additional probabilistic assumptions are introduced at this stage.

The lognormal distribution is parameterized by its mean and standard deviation, which are selected to represent the fragility characteristics of lines and poles. For overhead line outages, the mean and standard deviation are 3.8 and 0.122, respectively. For pole fragility curves, the corresponding parameters are 4.54 and 0.25, respectively [40].

Based on these probabilities, each component is stochastically assigned a failure state (failed or operational) using a Bernoulli trial.

The simulation is repeated over enough iterations to ensure statistical convergence. By aggregating the results of all iterations, the Monte-Carlo simulation provides an estimate of the likelihood and severity of the line's failures under certain windstorm speeds.

Since the disconnection of the substation poses the greatest challenge across all case studies, the simulations were exclusively on scenarios involving the outage of this link, resulting in the distribution network transitioning into an islanded microgrid. After this filtering, an additional step was performed to ensure that all remaining scenarios were unique, with no duplicates. The flowchart for the whole process can be seen in Fig. 2.

The output of this stochastic methodology is a prioritized set of failure scenarios that capture the most vulnerable states of the distribution network under high wind speeds. The most critical scenarios are carried forward to Section 4, where they serve to validate the proposed active and proactive resilience strategies.

3. Mathematical problem formulation

This section outlines the mathematical formulation of the model used in this study as a generalization model for identifying the techno-economic solutions for optimal operation of active distribution networks.

3.1. Objective function

The objective function described in Eq. (3) of the model aims to maximize the net priority weighted benefit of the restoration strategy by restoring the most critical loads while minimizing the reliance on DR programs. Specifically, it promotes the restoration of high-priority loads across the network and penalizes the use of DR blocks, which represent partial or full curtailment of lower-priority loads under contractual agreements. This balance ensures that critical infrastructure is prioritized in the restoration process, while DR is used efficiently and only when it provides a net benefit to overall system resilience. To ensure the model remains robust against physical limitations, like a depleted battery, the objective function includes a high-cost penalty index for disrupting supply. This penalty forces the model to consider service interruption as the absolute last resort. The last term in the objective function deals with the operational cost of generating units. In normal operation, without load curtailments, the objective function represents the social welfare maximization.

In short, the first term acts as a reward mechanism for restoring electrical loads of consumers. The second term introduces a penalty for utilizing demand response programs for low priority loads. The third term imposes a penalty for interrupting the supply to a load that was previously restored. Finally, the last term is the cost of power generation by the power generating units.

$$\begin{aligned} Max \sum_{t=1}^{T}\sum_{i\in L} \mathrm{Pr}_i^L\, \omega_{i,t}^L \Delta t - \sum_{t=1}^{T}\sum_{i\in\Lambda}\sum_{,d\in D_i} \mathrm{Pr}_i^L\, \mathrm{Pr}_{i,d,t}^{\mathrm{DR}}\, \omega_{i,d}^{\mathrm{DR}} \Delta t \\ - 1000\sum_{t=1}^{T}\sum_{i\in\Lambda} \sigma_{i,t}\Delta t - \sum_{t=1}^{T}\sum_{i\in \mathrm{G}} c_i^G P_{i,t}^G \Delta t \end{aligned} \quad (3)$$

In this function, the penalty factor associated with demand response activation serves as a numerical proxy for the unit compensation cost required to incentivize consumer participation. This 'pseudo-economic' weighting ensures that while the primary objective is the maximization of restored energy, the algorithm implicitly seeks a solution that minimizes the total contractual compensation costs incurred by the DSO.

3.2. Power Flow and nodal balance

The hourly active balance equations are provided in (4), while the reactive balance equations are provided in (5). It should be noted that, in this paper, the contribution of EES units in active power has been considered. In this case, the net power injection to each node has been presented, while the net power losses by the ongoing feeders have been implemented. Additionally, the served loads, $P_{i,t}^{LS}$ and $Q_{i,t}^{LS}$, have been considered to reflect the load shedding and demand response actions.

$$P_{i,t}^G + P_{k,t}^{Dchr} - P_{k,t}^{Chr} = P_{i,t}^{LS} + P_{ij,t}^{Loss} \quad \forall i, i \notin \Lambda \quad (4)$$

$$Q_{i,t}^G = Q_{i,t}^{LS} + Q_{ij,t}^{Loss} \quad \forall i, i \notin \Lambda \quad (5)$$

The nodal power balance equations are divided into two sets of constraints because of the need to differentiate DR allowed nodes from non-DR allowed. The electrical network operator must fulfill the active and reactive power balance by any means necessary, even if it's needed to perform a partial or full curtailment during contingent events. Based on the previous constraints, the nodal power balance includes the power injection from the substation and the generation into the distribution network, partial or full load curtailment, power through the lines, and power transferred to or discharged by the installed EES units. It should also be noted that the EES system can only provide active power in this model, like the power injection by the other DERs in this study.

3.3. Network topology and reconfiguration

According to the active and reactive power balance equations, the respective power losses can be expressed as (6) and (7), respectively, for active and reactive powers. The calculated power losses are valid for any operating scenarios, including normal and islanded mode operational planning scenarios [41].

$$P_{ij,t}^{Loss} = R_{ij} I_{ij,t}^2 \quad (6)$$

$$Q_{ij,t}^{Loss} = X_{ij} I_{ij,t}^2 \quad (7)$$

The voltage drops across the branches ij can be expressed as an

equality constraint for the normal power flow model. However, this constraint can be upgraded for the radial network with feeder reconfiguration possibilities, resulting in two complementary inequality constraints, provided in (8) and (9), compatible with normal and islanded mode operational studies [32].

$$V_{i,t}^2 - V_{j,t}^2 \geq 2\left(R_{ij}P_{ij,t} + X_{ij}Q_{ij,t}\right) + \left(Z_{ij}^2 I_{ij,t}^2\right) - \left(1 - y_{ij,t}\right)M \tag{8}$$

$$V_{i,t}^2 - V_{j,t}^2 \leq 2\left(R_{ij}P_{ij,t} + X_{ij}Q_{ij,t}\right) + \left(Z_{ij}^2 I_{ij,t}^2\right) + \left(1 - y_{ij,t}\right)M \tag{9}$$

The introduction of $y_{ij,t}$ is linked with the reconfiguration process, where the variable would be '1' if the branch is connected and '0' if the branch is open. In addition, to guarantee the functionality of this upgraded constraint, the Big-M method is applied with the use of the scalar M, which should be large enough to guarantee the functionality of the model. If $y_{ij,t} = 1$, the second term would be disregarded, and the voltage drop constraint would be activated. On the other hand, if $y_{ij,t} = 0$, the Big-M will guarantee the non-equality constraints. Analyzing the set of inequations, if there is a case of the connection between two nodes, the voltage drop is represented by the Kirchhoff Voltage Law (KVL).

The transmitted power through the branch ij is modeled as (10). In this case, the nodal voltage at the end of the line ij will be considered to model the power flow. Evidently, if there is no connection between bus i and bus j, the current flowing through the branch would be zero, modeled in (11) [42].

$$V_{j,t}^2 I_{ij,t}^2 = P_{ij,t}^2 + Q_{ij,t}^2 \tag{10}$$

$$0 \leq I_{ij,t}^2 \leq I_{ij}^{2,max} y_{ij,t} \tag{11}$$

In this regard, the bidirectional active and reactive power flows are modeled in (12) and (13), respectively. The corresponding binary variable for connected branches has been considered to guarantee the feasibility of the power flow constraints as well as the implementation of the Big-M method.

$$-y_{ij,t}P_{ij}^{max} \leq P_{ij,t} \leq y_{ij,t}P_{ij}^{max} \tag{12}$$

$$-y_{ij,t}Q_{ij}^{max} \leq Q_{ij,t} \leq y_{ij,t}Q_{ij}^{max} \tag{13}$$

In the distribution power flow problem, maintaining the voltage profile within the permissible bounds is an aspect to be maintained and necessary to enforce. Normally, the minimum value for a node's voltage is 0.9 pu, while the maximum value is 1.1 pu, as can be seen in (14).

$$V_i^{2,min} \leq V_{i,t}^2 \leq V_i^{2,max} \tag{14}$$

Since the nodal voltage is assumed to be a positive variable, the quadratic representation does not make the model more complex; therefore, the node's voltage constraint is provided in the quadratic statement [42].

3.4. Energy storage and distributed generation

The DG units considered for this study are modeled as dispatchable units, and the operating points of these units should be within the technical power generation limits, which are modeled in (15) and (16), for the active and reactive power of the dispatchable DGs, respectively. For the sake of simplicity, the unit commitment equations have been ignored in this study.

$$P_i^{G,min} \leq P_{i,t}^G \leq P_i^{G,max} \tag{15}$$

$$Q_{i,t}^{G,min} \leq Q_{i,t}^G \leq Q_{i,t}^{G,max} \tag{16}$$

Another notable observation is that it is assumed that the power flow from the upstream network to the distribution grid is unidirectional, and it is not possible to sell the surplus of local power generation to the upstream grid.

The intrinsic dynamic behavior of energy storage systems plays a key role and should be properly modeled over time. One important aspect is how the energy stored in the battery is represented, and this can be done using either the state of charge or the total stored energy. The energy stored in the battery can be represented as (17).

Additionally, since the problem is multi-temporal, the amount of stored energy is dependent on the energy stored in the previous period and the operation of the EES in charging or discharging modes. The efficiency of charging and discharging states is also considered [43].

$$E_{k,t}^{EES} = E_{k,t-1}^{EES} + \left(P_{k,t}^{Chr}\eta_k^{Chr} - \frac{P_{k,t}^{Dchr}}{\eta_k^{Dchr}}\right)\Delta t \qquad \forall t > 1 \tag{17}$$

To ensure the energy stored does not spiral into only charging or discharging, ignoring limits, Eq. (18) guarantees that the stored energy is within the permissible limits.

$$E_k^{min} \leq E_{k,t}^{EES} \leq E_k^{max} \tag{18}$$

Eqs. (19)–(21) are related to the power limits, more specifically regarding the charging and discharging, and the functionality of the battery's charging or discharging modes [43].

$$0 \leq P_{k,t}^{Chr} \leq P_t^{Chr,max} I_{k,t}^{Chr} \tag{19}$$

$$0 \leq P_{k,t}^{Dchr} \leq P_k^{Dchr,max} I_{k,t}^{Dchr} \tag{20}$$

$$0 \leq I_{k,t}^{Dchr} + I_{k,t}^{Chr} \leq 1 \tag{21}$$

Eqs. (19) and (20) are the limits for charging and discharging, and it should be noted that both equations have specific binary decision variables for charging and discharging modes, respectively. These two variables are to ensure that the EES is charging or discharging energy, and with the integration of (21), there is no possible way for a battery to be charging and discharging energy at the same time.

Additionally, the initial and final energy levels maintained in the battery system are expressed in (22) and (23), respectively. In this set of equations, the initial energy level for the battery system must be equal to a certain amount. However, the upper limit must not exceed a maximum amount of energy. It should be noted that the final energy stored in the battery, in normal operation, is usually considered to reach the initial stored energy. In contingent operational planning, this constraint can be relaxed to support the microgrid in maintaining more loads served.

$$E_{k,t_1}^{EES} = E_k^0 \tag{22}$$

$$E_{k,t_{24}}^{EES} \leq E_k^{max} \tag{23}$$

Under normal operation of the distribution network, the initial and final energy levels of the EES must be equal. Accordingly, Eq. (24) is used when simulating the system's normal operation with EES support.

$$E_{k,t_{24}}^{EES} = E_k^0 \tag{24}$$

As it was stated, LV and MV networks must always be operated in a radial topology. However, the operational topology can be changed for different seasons or when the main supply fails. When there's a change in the topology, the distribution network should remain radial for both grid-connected and islanded microgrids operation modes, and to guarantee this, a set of three constraints has been introduced in the literature [37]. Eq. (25) deals with the direction of the incidence matrix and the graph representation of the network. In this case, the binary decision variable $\vartheta_{ij,t}$ deals with the connection from node i to node j.

$$\vartheta_{ij,t} + \vartheta_{ji,t} = y_{ij,t} \tag{25}$$

For the reference bus at each part of the network, either grid-connected or islanded mode, with Eq. (26), it is not possible to inject the power from the network to the substation bus.

$$\sum_{j\in\Gamma_S}\vartheta_{ji,t}=0 \tag{26}$$

Eq. (27) confirms that the maximum power injection to a specific bus is limited to one link. This equation is proposed to avoid forming loops in the network topology while dealing with the total number of branches connected to each bus.

$$\sum_{j\in\Gamma_N}\vartheta_{ji,t}\le 1 \tag{27}$$

3.5. Demand Response and load prioritization

Regarding demand response constraints, there are typically two types of constraints: DR contracts and non-DR contracts. For the non-DR contracts, the status of all the loads in the distribution system can be '0' or '1', where '0' indicates a bus has not been restored and '1' indicates that the bus has been restored, as can be seen in (28) and (29), for the active and reactive power, respectively [36].

$$P_{i,t}^{LS}\ge\omega_{i,t}^{L}P_{i,t}^{LD}-P_{i,t}^{LC},\quad i\notin\Lambda \tag{28}$$

$$Q_{i,t}^{LS}=\omega_{i,t}^{L}Q_{i,t}^{LD} \tag{29}$$

The loads of private MGs with extra generation capacity must be restored, as that's a demand on their contract; therefore, the status of these loads must always be '1', as indicated in (30).

$$\omega_{i,t}^{LS}=1\quad\forall i\in EMG\backslash\Lambda \tag{30}$$

On the other hand, the DR contracted loads can be restored partially or fully as they don't have the same restrictions as the non-DR contract. Eqs. (31)–(32) represent the amount of active and reactive loads restored, respectively [36].

$$P_{i,t}^{LS}=P_{i,t}^{LD}-P_{i,t}^{DR}\qquad i\in\Lambda \tag{31}$$

$$Q_{i,t}^{LS}=Q_{i,t}^{LD}-\tan(\phi_i)\cdot P_{i,t}^{DR}\qquad i\in\Lambda \tag{32}$$

With the explanation of DR programs previously, the total DR contract of each load cannot be greater than its active power consumption. The summation of all DR blocks of said load mustn't be greater than the forecasted active power of the load as it is represented in (33).

$$\sum\nolimits_{d\in D_i}P_{i,d,t}^{DR,b}\le P_{i,t}^{LD}\quad\forall i\in\Lambda \tag{33}$$

The amount of applied DR for each load will be the summation of a portion of each DR block as it's shown in (34). To linearize the previous constraint, it can be replaced with (35)–(38) [36].

$$P_{i,t}^{DR}=\sum\nolimits_{d\in D_i}\gamma_{i,d,t}^{DR}\quad\forall i\in\Lambda \tag{34}$$

$$\gamma_{i,d,t}^{DR}\le P_{i,d,t}^{DR,b}\omega_{i,d,t}^{DR} \tag{35}$$

$$\gamma_{i,d,t}^{DR}\le\delta_{i,d,t}^{DR} \tag{36}$$

$$\gamma_{i,d,t}^{DR}\ge\delta_{i,d,t}^{DR}-P_{i,d,t}^{DR,b}\left(1-\omega_{i,d,t}^{DR}\right) \tag{37}$$

$$\gamma_{i,d,t}^{DR}\ge 0 \tag{38}$$

The amount applied from each load's DR block can't exceed the capacity of a single step, since each step comes at a higher price than the previous one. DR blocks should be used in order, starting with the cheaper steps first. This translates to, if a load uses the d^{th} step of its DR contract, it means all the earlier, less expensive steps must already be fully used, as modeled in (39).

$$\delta_{i,d,t}^{DR}\ge\omega_{i,(d+1),t}^{DR}P_{i,d,t}^{DR,b}\qquad\forall i\in\Lambda,d\in D_i\backslash\{n\} \tag{39}$$

The last two equations describe the status of the DR blocks. Eq. (40) indicates that if any DR block is used, the load is considered not restored. On the other hand, Eq. (41) shows that if none of the DR blocks are used, the load is fully restored, i.e., its status is '1'.

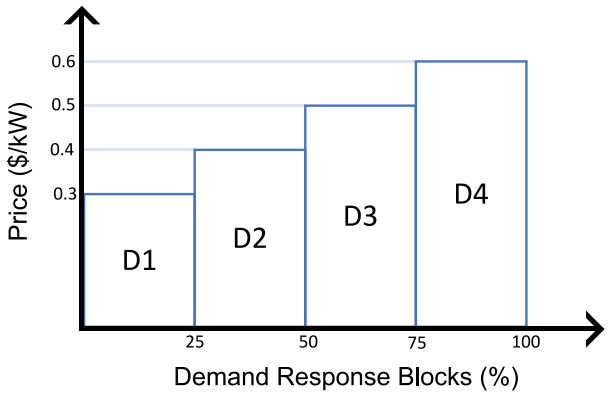

Fig. 3. DR programs in the load restoration phase [36].

$$\omega_{i,t}^{LS}\le 1-\omega_{id,t}^{DR}\qquad\forall i\in\Lambda,d\in D_i \tag{40}$$

$$\omega_{i,t}^{LS}\ge\sum\nolimits_{d\in D_i}\left(1-\omega_{id,t}^{DR}\right)-(n_d-1)\quad\forall i\in\Lambda \tag{41}$$

The representation of DR blocks is demonstrated in Fig. 3. As can be seen, the activation of DR blocks needs to be verified from the initial blocks, and the incremental cost will be applied for activating of more blocks. This strategy is particularly useful both during the event and after the event's scenario, where available supply may be limited and selective load curtailment can help prioritize critical loads.

Eq. (42) indicates that once a load is restored, it should ideally remain supplied. This means that if a load is restored previously, then it must stay restored at the next hour. This equation is relaxed with the ability to disrupt the continuity of the supply if it is only needed; otherwise, the objective function would receive a penalty.

$$\omega_{i,t}^{LS}+\sigma_{i,t}\ge\omega_{i,t-1}^{LS} \tag{42}$$

The ENS quantifies the difference between the total active load demand and the amount of load that is successfully restored at each bus, being defined in (43).

$$ENS=\sum\nolimits_{t=1}^{T}\sum\nolimits_{i\in\Lambda}\left(P_{i,t}^{LD}-P_{i,t}^{LS}\right)\Delta t \tag{43}$$

The hourly RI can be directly calculated according to the served loads, as stated in (44):

$$RI_t=1-\frac{\sum_{i\in\Lambda}\left(P_{i,t}^{LD}-P_{i,t}^{LS}\right)}{\sum_{i\in\Lambda}P_{i,t}^{LD}} \tag{44}$$

Regarding the association results between generation rescheduling, state of charge management of EES units, and demand response block activation, several considerations can be adjusted according to the preferences of network operators by selecting proper coefficients.

It should be highlighted that the loads have different priorities. In this case, the corresponding coefficients for high-, medium-, and low-priority loads are 100, 10, and 0.1, respectively. Additionally, the DR steps have different values, as shown in Fig. 3. Accordingly, grid-scale energy storage units are operated by the network operator to accommodate load serving during both normal and contingent events. Thus, activating the responsive loads would be the last resort before resorting to load-shedding actions. It should be noted that the costs of power production using local resources are considerably lower than those of corrective actions; therefore, generation rescheduling would be the first option to manage resources. Moreover, charging and discharging efficiencies are another issue that must be considered in the analysis.

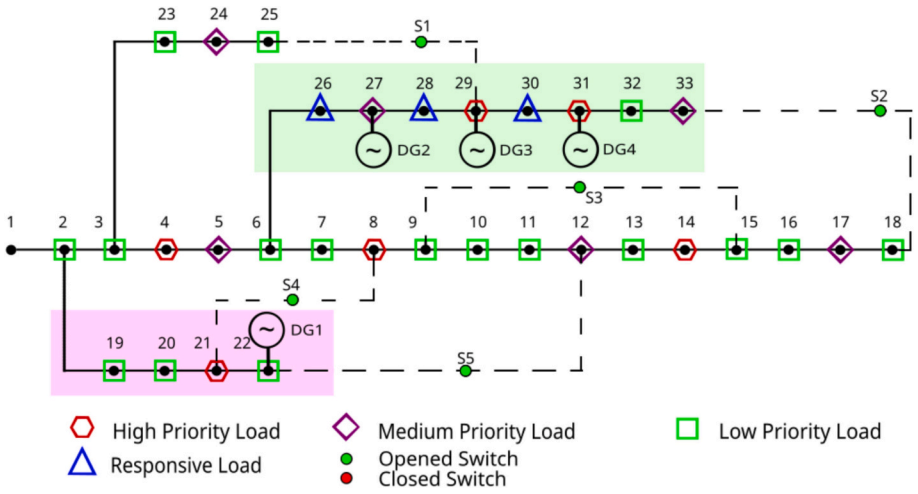

Fig. 4. Modified IEEE 33-bus system with DGs.

Table 2
Generating units' data in the modified IEEE 33-bus system.

Generator	Microgrid	Bus	Q^{max} (kVAr)	S^{max} (kVA)	c_i ($/kWh)	Type	Grid forming
Utility	–	1	3000	5000	0.010	Substation	Yes
DG1	MG2	22	50	100	0.005	Thermal	No
DG2	MG1	27	450	630	0.005	Thermal	Yes
DG3	MG1	29	0	425	0.005	PV	No
DG4	MG1	31	0	300	0.005	Wind	Yes

4. Simulation results

To evaluate the effectiveness of the developed MTOPF model, this section presents simulation results on modified IEEE 33-bus and 69-bus systems. Following the methodology established in Section 2, the study delves into their normal operation, worst scenario from the Monte-Carlo Simulations, and the implementation of EES to improve the resiliency of the networks studied.

For formulating, modelling, and solving the optimization problem, the General Algebraic Modelling System (GAMS) has been utilized on a Microsoft Surface 7 Pro with 16GB RAM and an Intel® Core™ i7-1065G7 Processor running Windows 11. The developed models have been implemented using MIQCP and CPLEX solver, under GAMS solver has been utilized to run the optimization problem.

4.1. IEEE 33-bus network

The first case study presented in this paper is the IEEE 33-bus network. The original network has 33 nodes, 32 links, and 5 switches, and the network data for the base case simulations are accessible from [17]. In this section, the simulation results are presented to validate the optimal power flow solution. The network is then modified by adding DERs and chronological loads for multi-temporal analysis. Then, the resilience assessment analysis is conducted to highlight the importance of network reconfiguration, operational planning in islanded mode, and forming the islanded microgrids. The simulation results for activating DRPs and the role of EESs are presented under various scenarios.

4.1.1. Original network results validation

The original network doesn't have any DERs. The total active and reactive power demands are 3.715 MW and 2.300 MVAr, respectively. In the original network, in its original topology, the minimum voltage is 0.913 pu at bus 18, while the voltage at the reference node is fixed to 1.0 pu. The total loss of the original network is 202.075 kW; while using network reconfiguration, the total loss is reduced to 139.160 kW, confirming the validation of the developed model for optimal power flow and network reconfiguration assessment [41].

Table 3
Generator output and power losses for the normal, reconfiguration, and reconfiguration with DGs in the modified IEEE 33-bus system.

	Normal operation	Reconfiguration	Reconfiguration with DGs
Power loss (kW)	202.075	139.160	58.131
Utility (kW)	3917.075	3854.160	2527.770
DG1 (kW)	–	–	86.602
DG2 (kW)	–	–	440.907
DG3 (kW)	–	–	422.048
DG4 (kW)	–	–	295.804

4.1.2. Normal operation strategy

The single-line diagram of the modified IEEE 33-bus system is illustrated in Fig. 4. As can be seen, the distributed generators have been placed on nodes 22, 27, 29, and 31, and the loads have been classified into low-, medium-, and high-priority loads.

The specifications of the generation units are presented in Table 2. There are two microgrids in this network, one privately owned and the other publicly owned. The privately owned microgrid includes three DGs, and the publicly owned microgrid contains one DG.

Generators with types such as “PV” and “Wind” are classified as non-dispatchable resources, as their output is fundamentally dependent on intermittent environmental profiles, such as solar irradiance and wind speed, respectively. Therefore, their scheduled active power output in the optimization model is strictly limited by the maximum available renewable energy resources at each hour. Thermal generators are classified as dispatchable resources, therefore their scheduled active power output in the optimization model is bounded by their limits and associated costs.

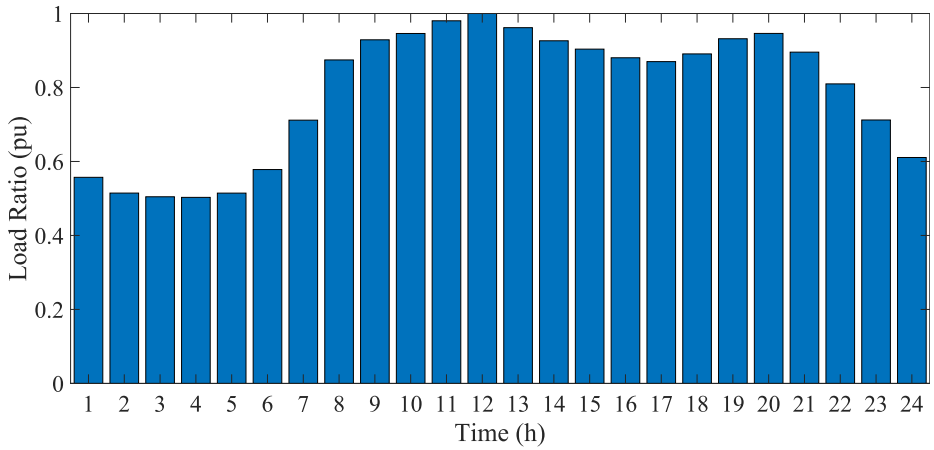

Fig. 5. Load profile for multi-temporal analysis in modified IEEE 33-bus [44].

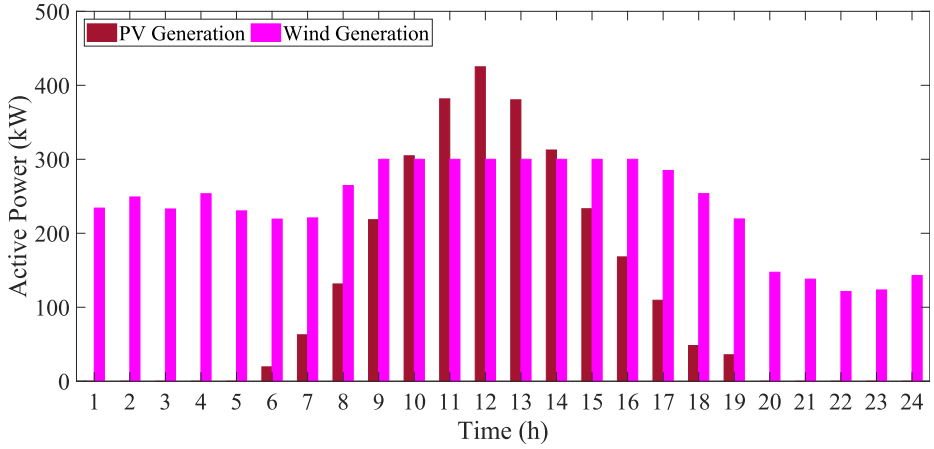

Fig. 6. PV and Wind generation profiles in modified IEEE 33-bus network [44].

Considering the specifications presented in Table 2, the network reconfiguration resulted in a considerable loss reduction in this studied network. The power loss has been reduced to 58.161 kW, which is significantly reduced compared to the original network design. The results for the validation case study are reported in Table 3.

In this case, the normal and reconfiguration studies in the original network, as well as the results in the presence of DG units, are provided in this table. It should be noted that, in the modified network, there are some responsive loads and different priorities to be served during contingent events. In this case, there are 6 nodes with high priority (4, 8, 14, 21, 29, 31), 6 nodes with medium priority (5, 12, 17, 24, 27, 33), and 20 nodes with low priority. In addition, there are 3 responsive loads at nodes 26, 28, and 30 participating in demand response actions.

For the multi-temporal analysis of the case study, a daily consumption profile has been extracted from E-Redes. This dataset corresponds to the 4200–00 Zip-Code (Paranhos, Porto, Portugal) for June 5th, 2023 [44]. The data obtained has been transformed into a load profile, as seen in Fig. 5. It should be noted that the chronological load profile is based on the real dataset, and the peak power is 3715 kW, according to the standard load of IEEE 33-bus test system. This profile has been used for the multi-temporal case studies investigated in this paper. The chronological profiles for the PV panel and the wind turbine are depicted in Fig. 6. Typically, PV output begins to rise shortly after sunrise, peaking around noon, and slowly diminishes by sunset. Wind energy presents a more variable and location-specific generation profile. Wind speeds are influenced by geography, weather patterns, and atmospheric conditions. In contrast to PV systems, wind turbines can operate at any time of the day or night.

4.1.3. Modified IEEE 33-bus network- HILP operation strategy with DGs

In this section, the optimal operation planning of the network under HILP events has been investigated. It should be noted that the private microgrid, MG1, accounts for eight nodes: four low-priority, two medium-priority, and two high-priority nodes. The public microgrid, MG2, accounts for four nodes, including three low-priority and one high-priority. While there is a difference between private and public microgrids, the public microgrid doesn't have any kind of contracts with the DSO, so they are not eligible for DR blocks management. The responsive

Table 4
Scenarios for the simulation of the modified IEEE 33-bus system.

	Scenario 1	Scenario 2	Scenario 3	Scenario 4	Scenario 5
Disconnected lines	01, 23, 29	01, 16, 31	01, 05, 22	01, 13, 17	01, 16, 25, 31
Total disconnected lines	3	3	3	3	4
ENS (kWh)	57,829.6	57,135.45	57,353.1	57,282.66	57,371.67

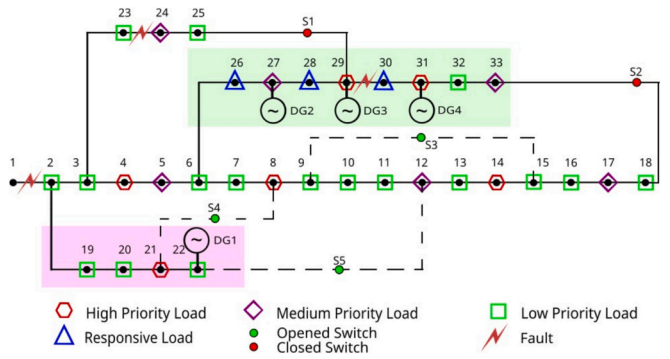

Fig. 7. Modified IEEE 33-bus system operating based on scenario 1.

Table 5
Activated DR blocks during the HILP event with DG units.

Time	Bus 26	Bus 28	Bus 30
1	(0,0,0,0)	(0,0,0,0)	(0,0,0,0)
2	(1,0,0,0)	(0,0,0,0)	(0,0,0,0)
3	(1)	(0,0,0,0)	(0,0,0,0)
4	(1)	(0,0,0,0)	(0,0,0,0)
5	(1,0,0,0)	(1,0,0,0)	(0,0,0,0)
6	(0,0,0,0)	(0,0,0,0)	(0,0,0,0)
7	(0,0,0,0)	(0,0,0,0)	(1,0,0,0)
8	(0,0,0,0)	(0,0,0,0)	(1,0,0,0)
9	(0,0,0,0)	(0,0,0,0)	(0,0,0,0)
10	(0,0,0,0)	(0,0,0,0)	(0,0,0,0)
11	(0,0,0,0)	(0,0,0,0)	(0,0,0,0)
12	(0,0,0,0)	(0,0,0,0)	(0,0,0,0)
13	(0,0,0,0)	(0,0,0,0)	(0,0,0,0)
14	(0,0,0,0)	(0,0,0,0)	(0,0,0,0)
15	(0,0,0,0)	(0,0,0,0)	(0,0,0,0)
16	(0,0,0,0)	(0,0,0,0)	(0,0,0,0)
17	(0,0,0,0)	(0,0,0,0)	(0,0,0,0)
18	(0,0,0,0)	(0,0,0,0)	(0,0,0,0)
19	(0,0,0,0)	(0,0,0,0)	(0,0,0,0)
20	(0,0,0,0)	(0,0,0,0)	(0,0,0,0)
21	(0,0,0,0)	(0,0,0,0)	(0,0,0,0)
22	(0,0,0,0)	(0,0,0,0)	(0,0,0,0)
23	(0,0,0,0)	(0,0,0,0)	(0,0,0,0)
24	(0,0,0,0)	(0,0,0,0)	(0,0,0,0)

loads in the private microgrid, i.e., nodes 26, 28, and 30, offer four DR blocks, each representing 25% of the total load. In other words, the DSO can utilize all DR blocks, effectively reducing the entire load if necessary. The priority factors associated with these DR blocks are 0.3, 0.4, 0.5, and 0.6, respectively, as seen in Fig. 3. With the implementation of the Monte-Carlo simulation in this study, many randomized scenarios have been generated to capture a wide range of possible operating conditions. To assess the most critical scenarios, the cases with the outages of the main substation have been chosen and ranked for the islanded mode operation scenario. Among 1000 Monte-Carlo generated cases, with the feature of main substation outage, and the elimination of duplicate scenarios, only 5 unique cases met the criteria for analysis. Table 4 summarizes the out-of-service lines that resulted in islanded microgrid formation.

Analyzing the results from this table, Scenario 1 has the worst performance, exhibiting the highest ENS value. Scenarios 5 and Scenario 3 also showed relatively poor performance, with an ENS close to that of Scenario 1. Thus, scenario 1 is objectively the worst, and it is investigated in this paper. The single-line diagram of this scenario with the faulty lines and network reconfiguration is illustrated in Fig. 7. It should be noted that with optimal switching actions, it is possible to form an islanded microgrid including all nodes, excluding node 1, and all DGs can contribute to serve demands.

Lines 23 and 29 are located near tie-switches, enabling network reconfiguration that prevents the formation of small, isolated islands.

Table 6
Unsupplied and supplied loads during HILP events with DG units.

Bus	Priority	Unsupplied load (kWh)	Unsupplied duration (h)	Supplied load (kWh)	Supplied duration (h)
2	Low	1895.206	24	0	0
3	Low	1705.686	24	0	0
4	High	1552.316	14	721.931	10
5	Medium	857.975	16	279.149	8
6	Low	1012.373	20	124.751	4
7	Low	3790.412	24	0	0
8	High	3033.902	17	756.51	7
9	Low	981.505	19	155.619	5
10	Low	1014.932	20	122.191	4
11	Low	806.537	22	46.306	2
12	Medium	910.171	17	226.953	7
13	Low	1137.124	24	0	0
14	High	1649.483	15	624.765	9
15	Low	476.56	9	660.563	15
16	Low	1014.932	20	122.191	4
17	Medium	286.029	5	851.094	19
18	Low	1705.686	24	0	0
19	Low	1705.686	24	0	0
20	Low	1705.686	24	0	0
21	High	435.071	5	1270.614	19
22	Low	1705.686	24	0	0
23	Low	1705.686	24	0	0
24	Medium	7959.866	24	0	0
25	Low	7959.866	24	0	0
26	Low	1060.906	22	76.218	24
27	Medium	0	0	1137.124	24
28	Low	1128.935	24	8.188	24
29	High	0	0	2274.247	24
30	Low	3704.633	24	85.78	24
31	High	0	0	2842.809	24
32	Low	3979.933	24	0	0
33	Medium	946.815	18	190.309	6
Overall *		57,829.6	17.97	12,577.31	8.22

* Unsupplied and Supplied duration hours are average.

Nevertheless, the fault on the three lines resulted in the creation of a fully connected, large islanded microgrid. However, the installed capacity is not sufficient to fulfill all loads. Thus, the load curtailment and activating the demand response are mandatory in this scenario. The activated blocks of responsive loads are provided in Table 5.

The final ENS and the availability of the nodes for this scenario can be seen from Table 6. The total energy supplied to the entire system equals 12,577.31 kWh accumulated over 24 h, having an average of 8.22 h with nodes of various priorities supplied. On the other hand, the total ENS for the entire system equals 57,829.6 kWh accumulated over 24 h, having an average of 17.97 h with nodes of various priorities not supplied.

4.1.4. Modified IEEE 33-bus network- HILP operation strategy with DGs and EESs

Following the analysis of the previous simulation results, the presented data highlights instances where the existing grid configuration proves insufficient in reliably meeting the demand at specific load points over 24 h. To address these deficiencies, an evaluation of the current grid topology has been conducted, and the results have been utilized for optimal management of the network planning studies. In this regard, buses with high or medium priority levels that are susceptible to supply-demand imbalance have been identified.

The strategy is to place the energy storage units for important nodes as a supplementary unit to serve these loads. Additionally, according to the initial simulations, bus 24 has the highest amount of energy not supplied, at 7959.866 kWh. Thus, the candidate buses for EES installations are 8, 14, and 24. Fig. 8 presents the buses with EES implementation and the microgrids to which they are currently assigned. Table 7 presents the characteristics of the EES installed in this case study. The activated DR blocks in this case study, with DG and EES units'

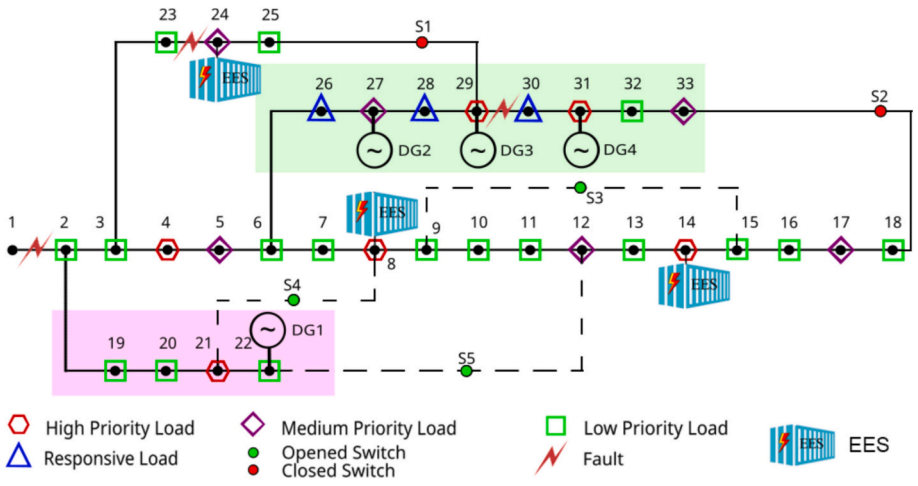

Fig. 8. Modified IEEE 33-bus system operating with EES.

Table 7
EES placement and characteristics in the modified IEEE 33-bus system.

EES unit	Bus	$_{P}Chr$ (kW)	$_{P}Dchr$ (kW)	$_{E}max$ (kWh)	$_{E}min$ (kWh)	$_{\eta}Chr$	$_{\eta}Dchr$	E_0 (kWh)
1	8	250	350	600	60	0.95	0.95	300
2	14	200	300	600	60	0.95	0.95	300
3	24	400	450	600	60	0.95	0.95	300

Table 8
Activated DR blocks during the HILP event with DG and EES units.

Time	Bus 26	Bus 28	Bus 30
1	(0,0,0,0)	(0,0,0,0)	(0,0,0,0)
2	(0,0,0,0)	(0,0,0,0)	(1)
3	(0,0,0,0)	(0,0,0,0)	(1)
4	(0,0,0,0)	(1,0,0,0)	(1,0,0,0)
5	(0,0,0,0)	(0,0,0,0)	(1)
6	(0,0,0,0)	(0,0,0,0)	(0,0,0,0)
7	(0,0,0,0)	(0,0,0,0)	(1,0,0,0)
8	(0,0,0,0)	(0,0,0,0)	(0,0,0,0)
9	(0,0,0,0)	(0,0,0,0)	(0,0,0,0)
10	(0,0,0,0)	(0,0,0,0)	(0,0,0,0)
11	(0,0,0,0)	(0,0,0,0)	(0,0,0,0)
12	(0,0,0,0)	(0,0,0,0)	(0,0,0,0)
13	(0,0,0,0)	(0,0,0,0)	(0,0,0,0)
14	(0,0,0,0)	(0,0,0,0)	(0,0,0,0)
15	(0,0,0,0)	(0,0,0,0)	(0,0,0,0)
16	(0,0,0,0)	(0,0,0,0)	(0,0,0,0)
17	(0,0,0,0)	(0,0,0,0)	(0,0,0,0)
18	(0,0,0,0)	(0,0,0,0)	(0,0,0,0)
19	(0,0,0,0)	(0,0,0,0)	(0,0,0,0)
20	(0,0,0,0)	(0,0,0,0)	(0,0,0,0)
21	(0,0,0,0)	(0,0,0,0)	(0,0,0,0)
22	(0,0,0,0)	(0,0,0,0)	(0,0,0,0)
23	(0,0,0,0)	(0,0,0,0)	(1,0,0,0)
24	(0,0,0,0)	(0,0,0,0)	(0,0,0,0)

Table 9
Unsupplied and supplied loads during HILP events with DG units.

Bus	Priority	Unsupplied load (kWh)	Unsupplied duration (h)	Supplied load (kWh)	Supplied duration (h)
2	Low	1895.206	24	0	0
3	Low	1705.686	24	0	0
4	High	1552.316	14	721.931	10
5	Medium	835.332	16	301.792	8
6	Low	1042.549	21	94.575	3
7	Low	3790.412	24	0	0
8	High	3033.902	17	756.51	7
9	Low	990.085	20	147.039	4
10	Low	1045.109	21	92.015	3
11	Low	852.843	24	0	0
12	Medium	867.47	17	269.654	7
13	Low	1137.124	24	0	0
14	High	1649.483	15	624.765	9
15	Low	559.206	11	577.918	13
16	Low	1045.109	21	92.015	3
17	Medium	338.849	6	798.275	18
18	Low	1705.686	24	0	0
19	Low	1705.686	24	0	0
20	Low	1705.686	24	0	0
21	High	435.071	5	1270.614	19
22	Low	1705.686	24	0	0
23	Low	1705.686	24	0	0
24	Medium	7748.632	23	211.234	1
25	Low	7959.866	24	0	0
26	Low	1136.799	24	0.324	24
27	Medium	0	0	1137.124	24
28	Low	1136.763	24	0.36	24
29	High	0	0	2274.247	24
30	Low	3407.314	21	383.099	24
31	High	0	0	2842.809	24
32	Low	3979.933	24	0	0
33	Medium	946.815	18	190.309	6
Overall *		57,620.3	18.16	12,786.61	8

* Unsupplied and supplied duration hours are average.

contribution, are presented in Table 8. It should be noted that the DR blocks are only activated in the private microgrid.

In comparison to the previous case, this scenario achieved an increase in supply for only three additional DR blocks, having a different outlook for all three buses. Analyzing the data by considering the DR status in two segments is not sufficient now, and that's because of bus 26 and bus 30 DR contributions. Bus 26 is now fully curtailed at every hour, passing the mantle of the bus with the highest energy supplied to bus 30, which had three full hours supplied and three partial supplies only reaching one DR block on the 4th, 7th, and 23rd hour. As for the other bus, bus 28, its DR supply did not change, as it was being supplied partially with only one block active, but the supply was anticipated by one hour.

The incorporation of the EES had a noticeable impact on the DR nodes, particularly on buses 26 and 30. However, the overall improvement in curtailment and supplied load was minimal, with only a 1% increase, making the global effect less significant. This outcome reflects the low priority assigned to the DR buses within the network. As these buses were not prioritized for supply, their curtailment levels remained high despite the EES implementation. This trend of full curtailment is the result of high demand by the system. Evidently, this case study uses

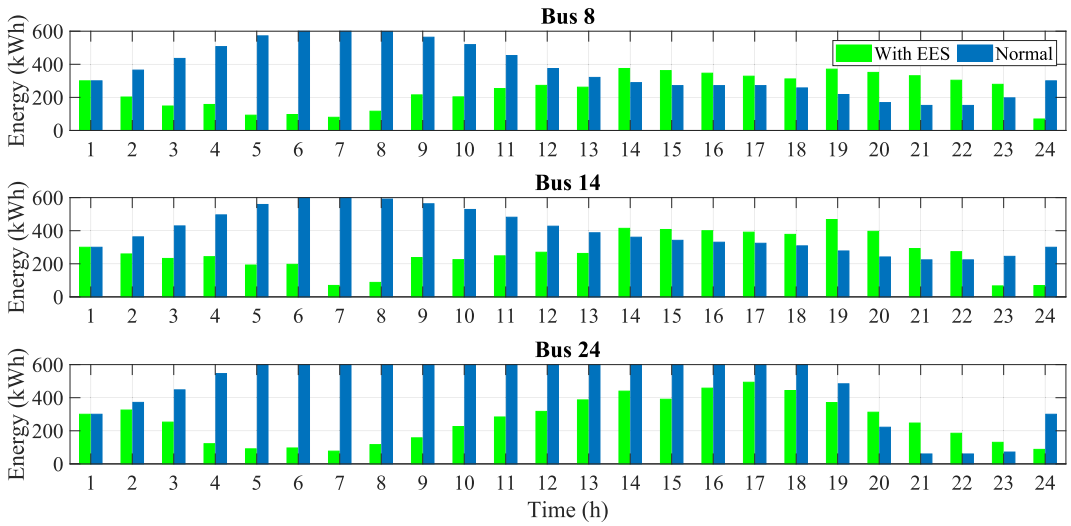

Fig. 9. Comparison of the energy stored in the EESs in normal and the HILP event.

real data, and at the time of the data's sampling, demand was high, as its load profile shows.

The final ENS and the availability of the nodes for this scenario can be seen from Table 9, the total energy supplied to the entire system equals 12,786.61 kWh for the given day, having an average of 8.00 h with nodes of various priorities supplied. On the other hand, the total ENS for the entire system equals 57,620.30 kWh, having an average of 18.16 h with nodes of various priorities not supplied.

Compared to the previous results, there was an increase in both the average duration of total supply and the total amount of load supplied. Additionally, the total ENS decreased while its duration increased. Regarding the high-priority buses, there was no observable impact on their ENS, which is significantly different from the medium-priority buses, as their ENS decreased. Noticeable improvements have been observed for bus 24, with one hour supply, making this bus not fully curtailed. Among the remaining buses, consisting of low-priority loads, their ENS increased. This is the result of both DR curtailment and the need to supply more energy for the higher priority buses, leading to curtailment for the other buses.

To better understand how EES performance varies depending on its location within the distribution network, an analysis has been conducted to examine the hourly energy profiles of these storage units in both normal operation planning and contingency event, as visualized in Fig. 9.

While EES units under normal operation prioritize economic optimization, under the contingency scenario, they adopt a common resilient oriented discharge-charge trajectory to maintain priority load supply. On the other hand, all the EES implemented for the normal operation scenario display similar charge-discharge patterns. The EES unit located at bus 8, starting from 300 kWh, initially discharges before gradually charging until it almost stabilizes. After this stabilization, a significant discharge overall occurs in the last hour, indicating sustained energy dispatch to meet demand. The initial discharge is seen on this EES unit, which leads to the conclusion that the network has high demand in the early hours of the day, and this EES unit meets the demand. This pattern is widely different for the contingency scenario from the pattern for normal operation. In the normal operation scenario, the EES unit charges early in the day to discharge a moderate portion around noon, ending by stabilizing until the last hour, where it charges again to coincide with the initial energy stored.

The EES located at bus 14, starting from 300 kWh, initially discharges before gradually charging until it almost stabilizes. After this stabilization, there's another period of charging and stabilization until the last few hours, where there's a discharge. This last hour pattern suggests that the network has high demand in the evening, as even the previous EES mentioned had a discharge at these hours. Reaching the same conclusion as the previous EES analysis, on normal operation, the EES charges steadily early in the day to discharge an insignificant

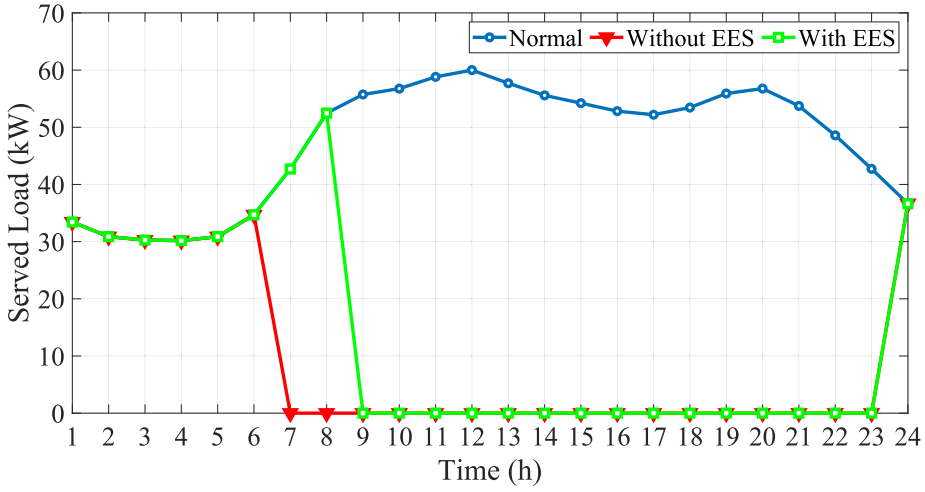

Fig. 10. Load serving capability for bus 12 with and without EES units in 33-bus system.

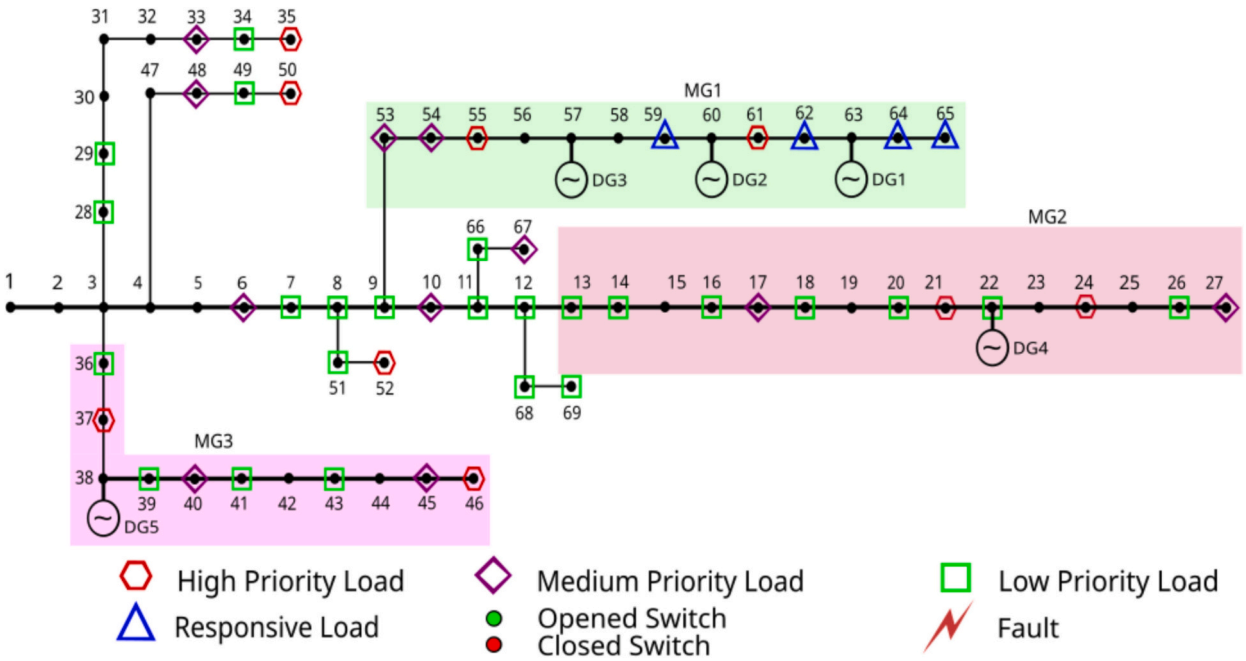

Fig. 11. Modified IEEE 69-bus system with DGs.

portion around noon, ending in stabilization. For the EES unit installed at bus 24, the initialization is approached from 300 kWh, has a pattern very similar to the other two EES units. This pattern is marked by the steep discharge early in the morning, followed by a steadily charging phase. However, the charging does not stabilize over time. Instead, after reaching its rated capacity, the EES begins a gradual discharge, forming a distinct pyramid-shaped profile. In contrast, under normal operation, the energy profile at this bus differs significantly from the others, characterized by a prolonged period of stabilized energy throughout most of the day, interrupted only by a steep discharge occurring late in the evening, where it charges again to coincide with the initial energy stored.

Analyzing all EES profiles, several supported conclusions can be drawn. First, the early hours of the day reflect high network demand, as evidenced by the consistent discharge observed across all EES units. Second, there is a notable increase in energy demand during the late evening, indicated by either a sharp or steady discharge of EES energy. Finally, during periods of normal operation, the EES rarely needs to supply energy to the buses, since their demand is largely met by other sources, as this is reflected in the prolonged periods of energy stabilization observed across the EES units.

Fig. 10 illustrates the serving capability of the network with and without the presence of EES units. As can be seen, the EES units installed in the network significantly improve the load serving capacity of the network for two more hours for bus 12 with a medium priority load.

4.2. IEEE 69-bus network

The second case study presented in this paper is the IEEE 69-bus network. The original network has 69 nodes, 68 links, and 5 switches, and the network data for the base case simulations are accessible from [17]. In this section, the simulation results are presented to validate the optimal power flow solution. The network is then modified by adding DERs and chronological loads for multi-temporal analysis like the modified IEEE 33-bus network. Then, the resilience assessment analysis is conducted to highlight the importance of network reconfiguration, operational planning in islanded mode, and forming the islanded microgrids. The simulation results for activating DRPs and the role of EESs are presented under various scenarios.

4.2.1. Original network results validation

The original network doesn't have any DERs. The total active and reactive power demands are 3.80219 MW and 2.6946 MVAr, respectively. In the original network, in its original topology, the minimum voltage is 0.9062 pu at bus 69, while the voltage at the reference node is fixed to 1.0 pu. The total loss of the original network is 224.99 kW; while using network reconfiguration, the total loss is reduced to 98.619 kW, confirming the validation of the developed model for optimal power flow and network reconfiguration assessment [45].

4.2.2. Normal operation strategy

The single-line diagram of the modified IEEE 69-bus system is illustrated in Fig. 11. As can be seen, the distributed generators have been placed on nodes 22, 38, 57, 60, and 63, and the loads have been classified into low-, medium-, and high-priority loads.

The specifications of the generation units are presented in Table 10. There are three microgrids in this network. In the modified network, there are three dispatchable DGs: DG1, DG4 and DG5 with the installed

Table 10
Generating units' data in the modified IEEE 69-bus system.

Generator	Microgrid	Bus	Q^{max} (kVAr)	S^{max} (kVA)	c_i ($/kWh)	Type	Grid forming
Utility	–	1	6000	8000	0.010	Substation	Yes
DG1	MG1	63	800	1130	0.005	Thermal	No
DG2	MG1	60	0	700	0.005	Wind	No
DG3	MG1	57	0	700	0.005	PV	Yes
DG4	MG2	22	100	150	0.005	Thermal	Yes
DG5	MG3	38	50	70	0.005	Thermal	Yes

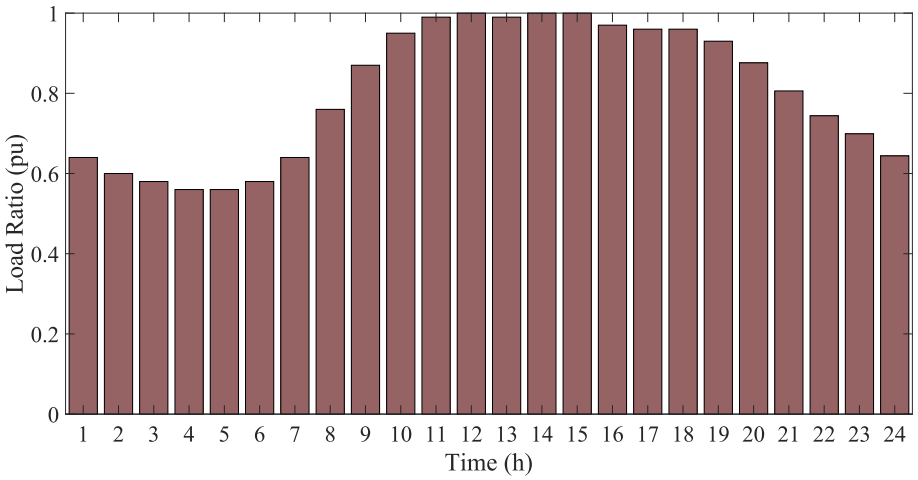

Fig. 12. Load profile for multi-temporal analysis in modified IEEE 69-bus.

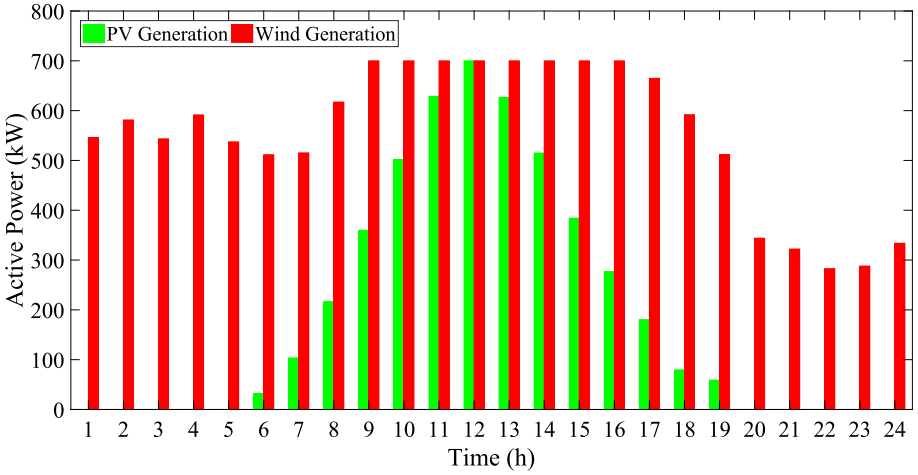

Fig. 13. PV and Wind generation profiles in modified IEEE 69-bus network.

Table 11
Generator output and power losses for the normal, reconfiguration, and reconfiguration with DGs in the modified IEEE 69-bus system.

	Normal operation	Reconfiguration	Reconfiguration with DGs
Power loss (kW)	224.993	98.619	17.563
Utility (kW)	4027.183	3900.808	1957.860
DG1 (kW)	–	–	798.014
DG2 (kW)	–	–	699.954
DG3 (kW)	–	–	203.357
DG4 (kW)	–	–	111.758
DG5 (kW)	–	–	48.809

capacity of 1130 kVA, 150 kVA and 70 kVA, respectively. In addition to the dispatchable units, a 700 kVA wind turbine and a PV park with the capacity of 700 kVA have been installed at buses 60 and 57, respectively.

Generators with types such as “PV” and “Wind” are classified as non-dispatchable resources, as their output is fundamentally dependent on intermittent environmental profiles, such as solar irradiance and wind speed, respectively. Therefore, their scheduled active power output in the optimization model is strictly limited by the maximum available renewable energy resources at each hour. Thermal generators are classified as dispatchable resources, therefore their scheduled active power output in the optimization model is bounded by their limits and associated costs. Fig. 12 presents the load profile for modified IEEE 69-bus test system, while the PV and Wind power generation profiles are illustrated in Fig. 13.

Considering the specifications presented in Table 11, the network reconfiguration resulted in a considerable loss reduction in this studied network. The power loss has been reduced to 17.563 kW, which is significantly reduced compared to the original network design. The results for the validation case study are reported in Table 8.

In this case, the normal and reconfiguration studies in the original network, as well as the results in the presence of DG units, are provided in this table. It should be noted that, in the modified network, there are some responsive loads and different priorities to be served during contingent events. In this case, there are 9 nodes with high priority (21, 24, 35, 37, 46, 50, 52, 55, 61), 11 medium priority (6, 10, 17, 27, 33, 40, 45, 48, 53, 54, 67), and 28 low priority nodes, including responsive loads at nodes 59, 62, 64, and 65 participating in demand response actions.

In this case study, the power generation profiles of renewable resources are different from the previous case study demonstrates a higher penetration of the non-dispatchable power injections. Additionally, the installed capacity of the non-dispatchable units is higher than the installed capacity of dispatchable DGs. It should be noted that the same strategy has been adopted for chronological load profile in this case study, while the peak power is 3.80219 MW.

Table 12
Scenarios for the simulation of the modified IEEE 69-bus system.

	Scenario 1	Scenario 2	Scenario 3	Scenario 4	Scenario 5	Scenario 6
Disconnected lines	1, 14, 20, 40, 41, 60	1, 64	1, 8, 52, 63	1, 5, 56	1, 13, 65	1, 49
Total disconnected lines	6	2	4	3	3	2
ENS (kWh)	33,145.60	32,895.83	32,847.20	32,734.45	32,795.82	32,672.85

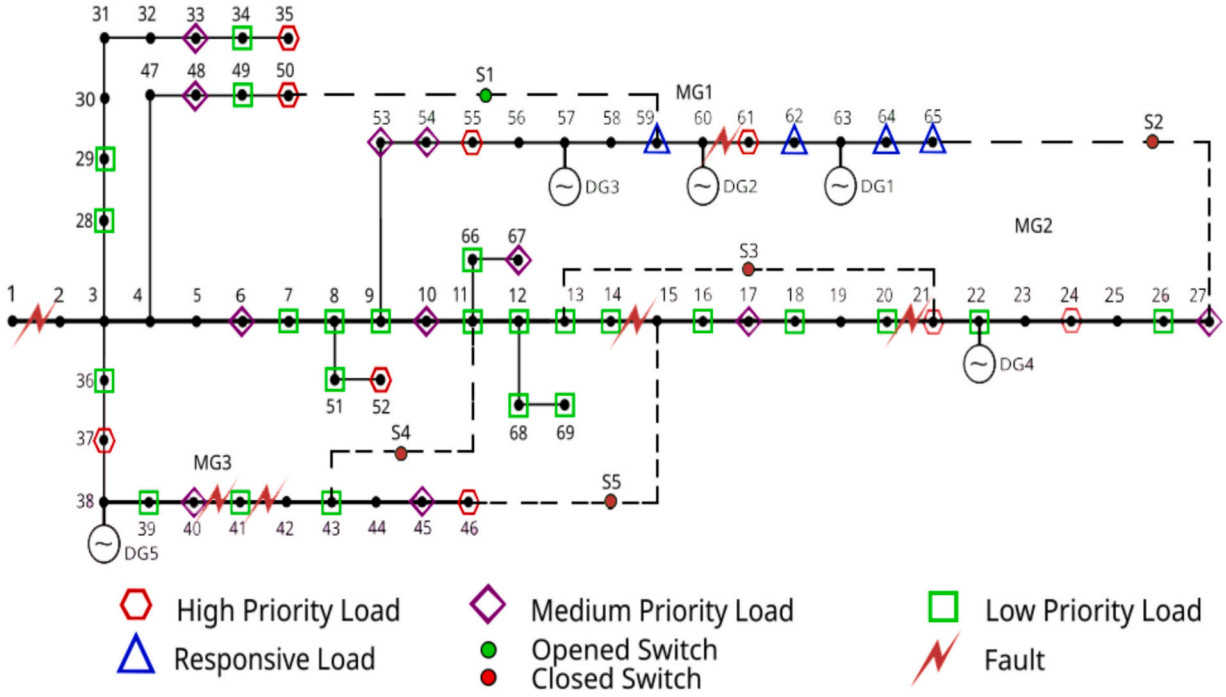

Fig. 14. Modified IEEE 69-bus system operating based on Scenario 1.

4.2.3. Modified IEEE 69-bus network- HILP operation strategy with DGs

In this section, the optimal operation planning of the network under HILP events has been investigated. There are three microgrids in this modified IEEE 69-bus distribution system, one privately owned (MG1) and the other two publicly owned (MG2 and MG3). The privately owned microgrid includes three DGs, i.e., DG1, DG2, and DG3, while the publicly owned MGs contain one DG each, as illustrated in Fig. 11.

Additionally, the private microgrid accounts for thirteen buses: five low-priority, two medium- priority, and two high-priority buses. Accumulatively, the public microgrids account for 26 buses, including 11 low-priority, 4 medium-priority loads, and 4 high-priority loads.

The responsive loads in the private microgrid, i.e., nodes 59, 62, 64, and 65, offer four DR blocks, each representing 25% of the total load. In other words, the DSO can utilize all DR blocks, effectively reducing the entire load if necessary. The priority factors associated with these DR blocks are 0.3, 0.4, 0.5, and 0.6, respectively, as seen in Fig. 3. With the implementation of the Monte-Carlo simulation in this study, many randomized scenarios have been generated to capture a wide range of possible operating conditions. To assess the most critical scenarios, the cases with the outages of the main substation have been chosen and ranked for the islanded mode operation scenario. Among 1000 Monte-Carlo generated cases, with the feature of main substation outage, and the elimination of duplicate scenarios, only 6 unique cases met the criteria for analysis. Table 12 summarizes the out-of-service lines that resulted in islanded microgrid formation.

Analyzing the results from the previous table, Scenario 1 performed the worst among all the options and had the highest ENS. In contrast, all the scenarios had ENS values that are relatively close to each other, with Scenario 6 being the case with lower ENS.

Table 13
Activated DR blocks during the HILP event with DG units.

Time	Bus 59	Bus 62	Bus 64	Bus 65
1	(0,0,0,0)	(1)	(0,0,0,0)	(1)
2	(0,0,0,0)	(1)	(0,0,0,0)	(1)
3	(0,0,0,0)	(1)	(0,0,0,0)	(1)
4	(1,0,0,0)	(0,0,0,0)	(0,0,0,0)	(1)
5	(1)	(0,0,0,0)	(0,0,0,0)	(1)
6	(0,0,0,0)	(0,0,0,0)	(0,0,0,0)	(1)
7	(0,0,0,0)	(0,0,0,0)	(0,0,0,0)	(1)
8	(0,0,0,0)	(0,0,0,0)	(0,0,0,0)	(1,1,0,0)
9	(0,0,0,0)	(0,0,0,0)	(0,0,0,0)	(0,0,0,0)
10	(0,0,0,0)	(0,0,0,0)	(0,0,0,0)	(0,0,0,0)
11	(0,0,0,0)	(0,0,0,0)	(0,0,0,0)	(0,0,0,0)
12	(0,0,0,0)	(0,0,0,0)	(0,0,0,0)	(0,0,0,0)
13	(0,0,0,0)	(0,0,0,0)	(0,0,0,0)	(0,0,0,0)
14	(0,0,0,0)	(0,0,0,0)	(0,0,0,0)	(0,0,0,0)
15	(0,0,0,0)	(0,0,0,0)	(0,0,0,0)	(0,0,0,0)
16	(0,0,0,0)	(0,0,0,0)	(0,0,0,0)	(0,0,0,0)
17	(1)	(1)	(1)	(1)
18	(0,0,0,0)	(0,0,0,0)	(0,0,0,0)	(0,0,0,0)
19	(1)	(1)	(0,0,0,0)	(1,1,1,0)
20	(1)	(1)	(0,0,0,0)	(1)
21	(1)	(1)	(0,0,0,0)	(1)
22	(1)	(1)	(0,0,0,0)	(1)
23	(1)	(1)	(1)	(1)
24	(0,0,0,0)	(0,0,0,0)	(0,0,0,0)	(0,0,0,0)

The single line diagram of the network under Scenario 1 is depicted in Fig. 14. In this scenario, two more switches should be opened to form the network as a radial distribution network, i.e., links 69 and 70 should be opened.

Table 14
Unsupplied and supplied loads during HILP events with DG units.

Bus	Priority	Unsupplied load (kWh)	Unsupplied duration (h)	Supplied load (kWh)	Supplied duration (h)
06	Medium	4.03	2	46.17	22
07	Low	613.51	18	166.57	6
08	Low	1262.18	21	186.00	3
09	Low	353.22	14	226.05	10
10	Medium	0.00	0	540.65	24
11	Low	2799.81	24	0.00	0
12	Low	2799.81	24	0.00	0
13	Low	36.59	5	117.88	19
14	Low	54.75	8	99.72	16
16	Low	664.76	18	213.80	6
17	Medium	156.84	3	1001.70	21
18	Low	1000.50	21	158.04	3
20	Low	0.96	1	18.35	23
21	High	0.00	0	2201.23	24
22	Low	20.16	5	82.18	19
24	High	0.00	0	540.65	24
26	Low	121.86	10	148.47	14
27	Medium	0.00	0	270.33	24
28	Low	274.92	12	227.11	12
29	Low	311.32	14	190.71	10
33	Medium	0.00	0	270.33	24
34	Low	162.90	10	213.62	14
35	High	0.00	0	115.85	24
36	Low	252.04	11	249.99	13
37	High	0.00	0	502.03	24
39	Low	296.83	15	166.58	9
40	Medium	46.32	2	417.10	22
41	Low	23.17	24	0.00	0
43	Low	21.44	4	94.41	20
45	Medium	140.17	4	617.13	20
46	High	0.00	0	757.30	24
48	Medium	361.35	5	1164.07	19
49	Low	7212.74	23	215.43	1
50	High	369.31	1	7058.86	23
51	Low	556.23	17	225.79	7
52	High	2.32	1	67.19	23
53	Medium	4.13	1	79.86	23
54	Medium	25.61	1	484.15	23
55	High	0.00	0	463.42	24
59	Low	1359.09	17	571.81	24
61	High	6238.66	6	17,781.74	18
62	Low	164.20	6	453.68	24
64	Low	4006.18	22	376.96	24
65	Low	589.03	12	550.20	24
66	Low	186.01	12	161.55	12
67	Medium	0.00	0	347.56	24
68	Low	317.35	13	223.30	11
69	Low	335.27	14	205.38	10
Overall *		33,145.60	8.77	40,270.89	16.42

* Unsupplied and Supplied duration hours are average.

This switching action enables network reconfiguration that prevents the formation of small, isolated microgrids resulting in a big microgrid works in an islanded mode and can serve the loads as much as possible. However, the installed capacity is not sufficient to fulfill all loads. Thus, the load curtailment and activating the demand response are mandatory in this scenario. The activated blocks of responsive loads are provided in Table 13.

The final ENS and the availability of the nodes for this scenario can be seen from Table 14. The total energy supplied to the entire system equals 40,270.89 kWh accumulated over 24 h, having an average of 16.42 h with nodes of various priorities supplied. On the other hand, the total ENS for the entire system equals 33,145.60 kWh accumulated over 24 h, having an average of 8.77 h with nodes of various priorities not supplied.

Regarding the high priority buses, only three buses were not entirely supplied, being bus 50, 51 and 61, with outages of 1 or 6 h. The medium priority buses had similar results, with 4 buses supplied completely with the rest of the medium priority buses, experiencing outages ranging from 1 h to 5 h. Among the remaining buses, 3 out of 29 buses were not fully supplied. These results still validate the priority given to all loads and their ranking in the power distribution hierarchy.

4.2.4. *Modified IEEE 69-bus network- HILP operation strategy with DGs and EESs*

Following the analysis of the previous simulation results, the presented data highlights instances where the existing grid configuration proves insufficient in reliably meeting the demand at specific load points over 24 h. To address these deficiencies, an evaluation of the current grid topology must be done and to do so it's needed to identify buses with high or medium priority levels which are susceptible to supply-demand imbalance.

According to Table 14, bus 61, has high priority and has the highest not supplied load. For the medium priority buses, all of those who were not fully supplied have low ENS. However, bus 48 and bus 17, despite having a low unsupplied load and duration, may also warrant attention due to their priority status. Therefore, these three buses are considered suitable candidates for EES deployment. Fig. 15 presents the buses with EES implementation and the microgrids to which they are currently assigned. Table 15 presents the characteristics of the EES units alongside what bus they are connected to.

Similar to the analysis previously conducted on the modified IEEE 33-bus system, upon detecting a disturbance on the network, the private microgrid activates the DR protocols to curtail eligible loads. The curtailment occurred during some hours of the sample time, as shown in Table 16.

Approximately 65% of the private microgrid load has been classified as curtailable, while approximately 35% of the load has been supplied. When compared to topology without EES implementation, the changes observed are visible.

The first bus with DR contract, bus 59 showed intermittent operation, remaining completely supplied during early hours (1st-6th) except for a brief full load supply at 3rd hour. From 7th to 24th hours, it was fully curtailed.

Bus 62 maintained continuous full operation until the 15th hour, and after that it was fully curtailed until the last hour.

On the other hand, bus 64 remained almost entirely curtailed, with just one notable exception: a single-block supply at the first hour. Lastly, bus 65 mirrored Bus 62's operational pattern.

The incorporation of the EES had a noticeable impact on the DR buses. The overall load pattern didn't remain largely consistent with the behavior observed without EES integration and the percentage of curtailments increased. These changes of percentage compared to the scenario without EES integration are result of the system redirecting energy for higher priority buses with load's demand. This conclusion on the analysis of the DR blocks, is almost the same as the conclusion reached on the 33-bus system. The final ENS and the availability of the buses for this scenario can be seen from Table 17.

The total energy supplied to the entire system equals 41,944.42 kWh accumulated over 24 h, having an average of 13.52 h with buses of various priorities supplied. On the other hand, the total ENS for the entire system equals 31,472.07 kWh accumulated over 24 h, having an average of 11.77 h with buses of various priorities not supplied.

Compared to the previous results, there was a decrease in the average duration of total supply and an increase in the average duration of ENS. The average of hours may have increased but this increase comes from priority, and the selection of what buses needed supply.

Regarding the high-priority buses, there was an observable impact on their performance with respect to the unsupplied duration and load. When there was no implementation of EES, only three buses with unsupplied load. However, with the implementation of EES, every single high priority bus was supplied.

This improvement on high priority buses comes from the setback of load supply on the medium- priority buses. With the implementation of EES there are more buses with supplied load but with more hours,

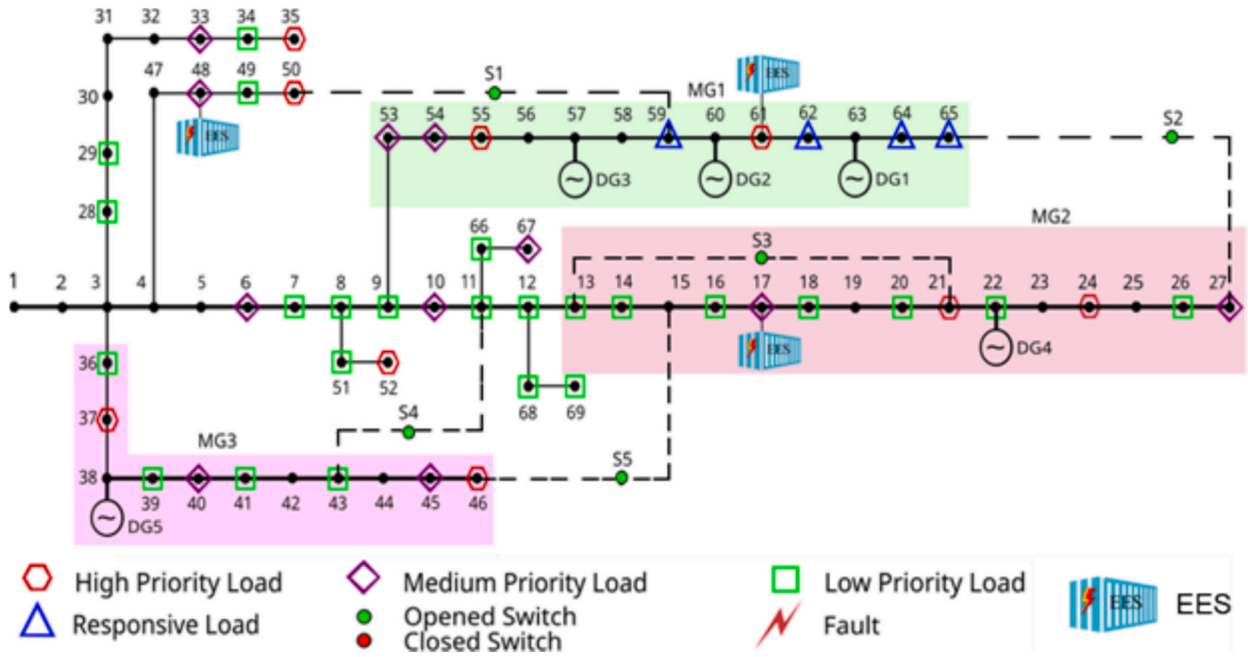

Fig. 15. Modified IEEE 69-bus system operating with EES.

Table 15
EES placement and characteristics in the modified IEEE 69-bus system.

EES unit	Bus	$_{P}Chr$ (kW)	$_{P}Dchr$ (kW)	$_{E}max$ (kWh)	$_{E}min$ (kWh)	$_{\eta}Chr$	$_{\eta}Dchr$	E_0 (kWh)
1	61	900	1100	1500	150	0.9	0.9	750
2	48	360	380	400	9.5	0.9	0.9	200
3	17	410	430	450	7.2	0.9	0.9	225

Table 16
Activated DR blocks during the HILP event with DG and EES units.

Time	Bus 59	Bus 62	Bus 64	Bus 65
1	(1)	(1)	(1)	(1)
2	(1)	(1)	(0,0,0,0)	(1)
3	(0,0,0,0)	(1)	(0,0,0,0)	(1)
4	(1)	(1)	(0,0,0,0)	(1)
5	(1)	(1)	(0,0,0,0)	(1)
6	(1)	(1)	(0,0,0,0)	(1)
7	(0,0,0,0)	(1)	(0,0,0,0)	(1)
8	(0,0,0,0)	(1)	(0,0,0,0)	(1)
9	(0,0,0,0)	(1)	(0,0,0,0)	(1)
10	(0,0,0,0)	(1)	(0,0,0,0)	(1)
11	(0,0,0,0)	(1)	(0,0,0,0)	(1)
12	(0,0,0,0)	(1)	(0,0,0,0)	(1)
13	(0,0,0,0)	(1)	(0,0,0,0)	(1)
14	(0,0,0,0)	(1)	(0,0,0,0)	(1)
15	(0,0,0,0)	(0,0,0,0)	(0,0,0,0)	(0,0,0,0)
16	(0,0,0,0)	(0,0,0,0)	(0,0,0,0)	(0,0,0,0)
17	(0,0,0,0)	(0,0,0,0)	(0,0,0,0)	(0,0,0,0)
18	(0,0,0,0)	(0,0,0,0)	(0,0,0,0)	(0,0,0,0)
19	(0,0,0,0)	(0,0,0,0)	(0,0,0,0)	(0,0,0,0)
20	(0,0,0,0)	(0,0,0,0)	(0,0,0,0)	(0,0,0,0)
21	(0,0,0,0)	(0,0,0,0)	(0,0,0,0)	(0,0,0,0)
22	(0,0,0,0)	(0,0,0,0)	(0,0,0,0)	(0,0,0,0)
23	(0,0,0,0)	(0,0,0,0)	(0,0,0,0)	(0,0,0,0)
24	(0,0,0,0)	(0,0,0,0)	(0,0,0,0)	(0,0,0,0)

contributing to an increase in ENS for the medium buses. Among the remaining buses, an increase of ENS was seen, validating that the use of EES can decrease ENS focusing on priority driven loads.

To better understand how EES performance varies depending on its location within a distribution, it is done an analysis examining the temporal energy profiles of these storage units, visualized in Fig. 16.

The EES located on bus 61, starting at 750 kWh, gradually charges until it almost stabilizes at the 9th hour. After this stabilization, a gradual discharge overall occurs, reaching its lowest in the final hour. This pattern is widely different from the pattern for normal operation. On the normal operation, the EES charges early in the day to discharge a moderate portion on the last hours of the day, ending stabilizing to coincide with the initial energy stored.

The EES located on bus 48, starting at 200 kWh, initially stabilized for nine hours before gradually charging until a stabilization occurs. After this stabilization, there's a steep discharge followed by a gradual discharge until the last hour. This behavior suggests that the network has high demand late in the evening and low demand from this ESS in the early morning and early afternoon. On the other hand, on normal operation, the EES charges steadily early in the day ending stabilizing for most hours only to discharging some energy into the network so that the final energy stored could be equal to the initial energy stored. The last EES to be analyzed, located on bus 17 and starting at 225 kWh, has a pattern very similar to the last EES unit. This pattern is marked by stabilization early in the morning, followed by a gradual charge until it stabilizes and ends with a gradual discharging phase. In contrast, under normal operation, the energy profile at this bus differs significantly from the others, characterized by a prolonged period of stabilized energy throughout most of early morning, interrupted only by a steep discharge occurring late in the morning where it coincides with the initial energy stored.

Analyzing all EES profiles, several supported conclusions, consistent with the findings in the modified IEEE 33-bus system, can be drawn. First, the early hours of the day reflect low network demand, as evidenced by the consistent gradual charging phase observed across the first EES unit and the stabilizations of the other EES units. Second, there is a notable increase in energy demand during the late evening, indicated by either a sharp or steady discharge in the EES profiles. Finally, during periods of normal operation, the EES rarely needs to supply energy to the buses, since their demand is largely met by other sources, as this is reflected in the prolonged periods of energy stabilization observed across the EES units.

Fig. 17 illustrates the serving capability of the network with and without the presence of EES units. As can be seen, the EES units installed

Table 17
Unsupplied and supplied loads during HILP events with DG and EES units.

Bus	Priority	Unsupplied load (kWh)	Unsupplied duration (h)	Supplied load (kWh)	Supplied duration (h)
06	Medium	0	0	50.2034	24
07	Low	754.2276	23	25.856	1
08	Low	1400.175	23	48	1
09	Low	454.47	17	124.8	7
10	Medium	522.62	23	18.032	1
11	Low	2707.005	23	92.8	1
12	Low	2707.005	23	92.8	1
13	Low	68.712	10	85.76	14
14	Low	60.712	9	93.76	15
16	Low	849.4395	23	29.12	1
17	Medium	1158.54	24	0	0
18	Low	1120.14	23	38.4	1
20	Low	6.246	7	13.063	17
21	High	0	0	2201.226	24
22	Low	43.1897	10	59.148	14
24	High	0	0	540.652	24
26	Low	106.246	9	164.08	15
27	Medium	0	0	270.326	24
28	Low	374.114	16	127.92	8
29	Low	374.114	16	127.92	8
33	Medium	0	0	270.326	24
34	Low	186.9855	11	189.54	13
35	High	0	0	115.854	24
36	Low	374.114	16	127.92	8
37	High	0	0	502.034	24
39	Low	324.456	15	138.96	9
40	Medium	0	0	463.416	24
41	Low	23.1708	24	0	0
43	Low	45.534	9	70.32	15
45	Medium	675.44684	21	81.85214	3
46	High	0	0	757.29898	24
48	Medium	1525.411	24	0	0
49	Low	7181.9643	23	246.208	1
50	High	0	0	7428.1723	24
51	Low	756.0945	23	25.92	1
52	High	0	0	69.5124	24
53	Medium	55.2015	16	28.79265	8
54	Medium	0	0	509.7576	24
55	High	0	0	463.416	24
59	Low	1636.89524	19	294.00476	24
61	High	0	0	24,020.396	24
62	Low	274.84727	10	343.04073	24
64	Low	4237.85733	23	145.28567	24
65	Low	506.75026	10	632.48074	24
66	Low	154.602	10	192.96	14
67	Medium	0	0	347.562	24
68	Low	402.892	16	137.76	8
69	Low	402.892	16	137.76	8
Overall *		31,472.07	11.77	41,944.42	13.52

* Unsupplied and Supplied duration hours are average.

in the network significantly improve the load serving capacity of the network for six more hours for bus 61 with a high priority load.

4.3. Sensitivity analysis

To highlight the importance of the EES units' contribution to enhancing the resilience of the distribution networks studied in this paper, a sensitivity analysis has been conducted in this section. In this regard, the location of the EES units remains fixed, while the rated capacity has been changed. For instance, 100% means that the original values have been reflected in the previous sections, and 0% means that there is no EES unit installed, as discussed in the previous section. It should be noted that the total installed capacity in the modified IEEE 33-bus and modified IEEE 69-bus networks is 1800 kWh and 2350 kWh, respectively. It is evident that increasing the size of the EES units will decrease the ENS. The results are presented in Table 18.

4.4. Computational complexity

The optimization problem includes both binary and continuous decision variables. Binary variables represent network reconfiguration, demand response activation, load curtailment, and energy storage operating modes. Continuous variables represent power generation, power flows, nodal voltages, load restoration, and energy storage operation. For the modified IEEE 33-bus system, which has 37 lines, 4 distributed generators, and 3 energy storage units, the model involves approximately 1320 binary variables and 2000 continuous variables, leading to a total of roughly 3320 variables. In the modified IEEE 69-bus system, with 74 lines and 5 distributed generators, the problem expands substantially to an estimated 2232 binary variables and 3636 continuous variables, totaling approximately 5868 variables.

4.5. Demand response awareness

From a technical-economic perspective, the results demonstrate the model's ability to selectively activate DR blocks based on their priority and impact on system recovery. The optimization effectively balances the technical necessity of load restoration with the economic constraint of minimizing expensive emergency interventions. This demonstrates that a resilience-centric approach, when governed by hierarchical penalty factors, naturally aligns with the economic objective of reducing operational expenditures during HILP events.

5. Concluding remarks

In this paper, both active and proactive strategies have been implemented to enhance the interoperability of distribution networks in the presence of DERs. The active strategies include optimal operation of DERs, network reconfiguration for the purpose of loss reduction for normal operation, and islanded microgrid formations during the contingent events. The generation rescheduling of dispatchable DERs, including DGs and EESs, is another feature of active strategies that has been considered in this study. The situational awareness resulting from the Monte-Carlo Simulations and preparedness activities, including determination of fragile feeders, load prioritization, and demand response contracts, are some examples of the proactive actions made to enhance the resiliency of the network in the occurrence of contingency events. Enhancing the Interoperability of Smart Grids with Active and Proactive Strategies. In this regard, this study explores a comprehensive study on how the resilience of active distribution networks can be leveraged by proper decision making, optimal network recognition, and implementation of demand response actions. The simulation results on the modified IEEE 33-bus network are demonstrated in this paper to highlight the importance of both active and proactive actions. In addition, using different case studies and scenarios, the performance of EES units and network reconfiguration strategies has been demonstrated how the developed model effectively improves load-serving capability and the resilience index, particularly for high- and medium-priority loads, while minimizing the impact on lower-priority consumers. It should be noted that the developed model is a multi-disciplinary framework for MTOPF applications in both normal and contingent events. Under normal operating conditions, network reconfiguration alone decreased losses, and the strategic operational scheduling of DGs drove losses even further down. These results prove that with the increase of strategically placed DGs, the losses and operational cost of the network decrease. In the catastrophic events and natural hazards, the network operation challenge is to minimize the load shedding and reduce the number of affected customers, minimize the ENS, and recover the network to the normal situation. Indeed, the proposed strategy contributes to the development of flexible, interoperable, and resilient distribution networks, aligning with the evolving requirements of future smart grids that integrate diverse energy resources and consumer participation.

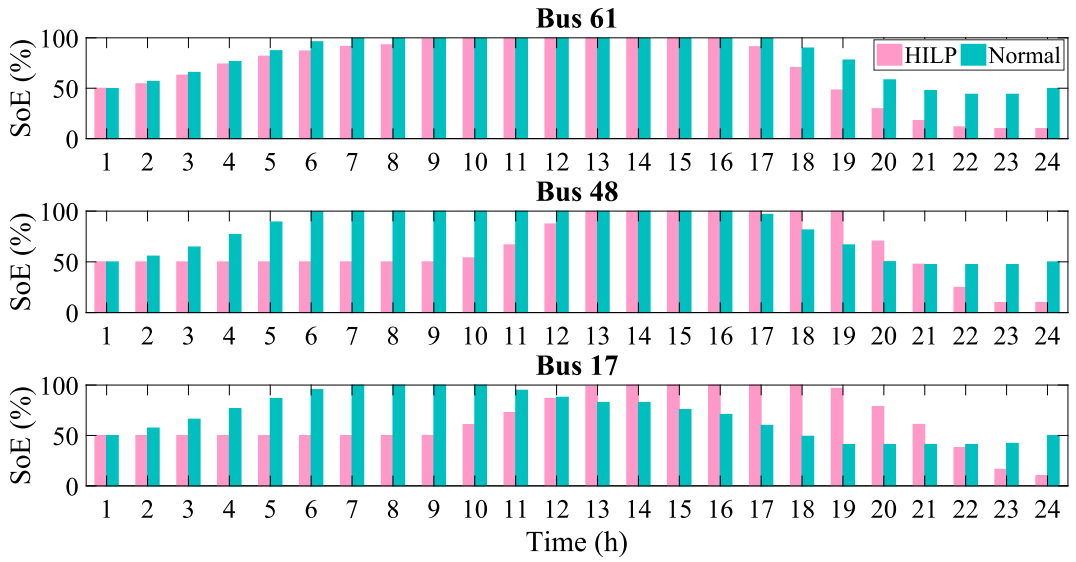

Fig. 16. Comparison of state of energy (SoE) of the EES units in modified IEEE 69-bus system.

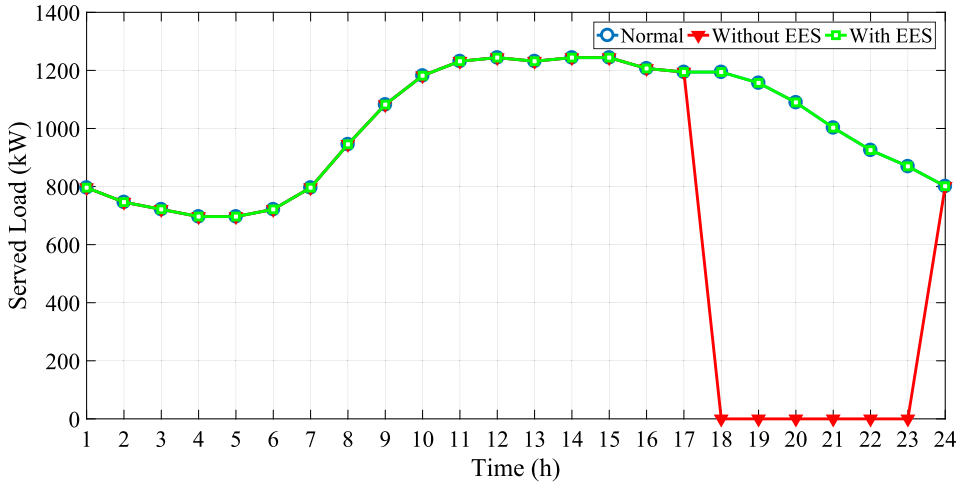

Fig. 17. Load serving capability for bus 61 with and without EES units in 69-bus system.

Table 18
Sensitivity analysis of system response (ENS) to changes in EES capacity.

Installed EES (%)	0	50%	100%*	150%	200%
Modified IEEE 33-Bus	57,829.60 kWh	57,754.51 kWh	57,620.30 kWh	49,802.78 kWh	48,884.43 kWh
Modified IEEE 69-Bus	33,145.60 kWh	32,652.61 kWh	31,472.07 kWh	31,092.35 kWh	30,683.62 kWh

* In the modified IEEE 33-bus system, 100% equal to 600 kWh + 600 kWh + 600 kWh = 1800 kWh.
* In the modified IEEE 69-bus system, 100% equal to 1500 kWh + 400 kWh + 450 kWh =2350 kWh.

In addition to the qualitative discussion above, the results obtained in this work also demonstrate clear quantitative improvements in system performance. In particular, the proposed framework leads to a reduction in ENS under HILP scenarios, with ENS decreasing from 57.8 MWh to 57.6 MWh in the IEEE 33-bus system and from 33.1 MWh to 31.5 MWh in the IEEE 69-bus system under worst-case conditions. Moreover, the inclusion of EES results in an increase in the average RI, improving from 30% to 32% in the 33-bus network and from 55% to 58% in the 69-bus network, highlighting the stronger resilience gains achieved in larger networks.

Despite the effectiveness of the proposed methodology, some limitations must be acknowledged. The mixed-integer and multi-temporal nature of the optimization problem increases computational complexity, particularly as the number of buses, time steps, and Monte-Carlo scenarios grows. Furthermore, the accuracy of the results depends on the assumed fragility curves and probabilistic modelling of component failures, which may not fully capture regional or asset-specific characteristics.

This work paves the way for several future developments, including the integration of artificial intelligence in the modelling and decision-making phase to reduce the computational burden and help the network operators in real-world situations. Other possible advances include optimizing the redundancy assessment, strategic hardening of the network assets, and automating the placement of the EES units, including both mobile and stationary batteries.

While the current study successfully validates a resilience-oriented restoration strategy using priority-based penalties, future work could expand this framework into a formal bi-objective technical-economic optimization model. Such an evolution would involve the generation of

optimal fronts to explicitly analyze the trade-off between the monetary cost of DR compensation and the ENS.

CRediT authorship contribution statement

Diogo Filipe Azevedo Souto Ramos: Writing – original draft, Visualization, Software, Methodology, Conceptualization. **Mohammad Sadegh Javadi:** Writing – review & editing, Validation, Supervision, Methodology, Investigation, Data curation.

Declaration of competing interest

The authors declare that they have no known competing financial interests or personal relationships that could have appeared to influence the work reported in this paper.

Acknowledgments

Mohammad Sadegh Javadi acknowledges support from the EU Horizon Europe Programme under GA ID: 101230578 (INNO-TREC Project; DOI: 10.3030/101230578) and from COMPETE2030-FEDER-00883700 and FCT (INVINCIBLE Project; DOI: 10.54499/2023.17788.ICDT).

Data availability

Data will be made available on request.

References

[1] F. Ghanavati, G.J. Osório, J.C.O. Matias, J.P.S. Catalão, Transactive data-driven and consumer-centric home energy management system for local energy communities in Portugal, Sustain. Cities Soc. 131 (Sep. 2025) 106698, https://doi.org/10.1016/J.SCS.2025.106698.
[2] O.O. Ademulegun, D. Flynn, N.J. Hewitt, Designing tariff for charging electric vehicles at home with equity in mind – the tripartite tariff, Sustain. Cities Soc. 118 (Jan. 2025) 106018, https://doi.org/10.1016/J.SCS.2024.106018.
[3] J.L. Meirinhos, D.E. Rua, L.M. Carvalho, A.G. Madureira, Multi-temporal optimal power flow for voltage control in MV networks using distributed energy resources, Electr. Power Syst. Res. 146 (May 2017) 25–32, https://doi.org/10.1016/J.EPSR.2017.01.016.
[4] J. Mello, J. Villar, Integrating flexibility and energy local markets with wholesale balancing responsibilities in the context of renewable energy communities, Energy 282 (Nov. 2023) 128853, https://doi.org/10.1016/J.ENERGY.2023.128853.
[5] E. Kuznetsova, M.A. Cardin, M. Diao, S. Zhang, Integrated decision-support methodology for combined centralized-decentralized waste-to-energy management systems design, Renew. Sust. Energ. Rev. 103 (Apr. 2019) 477–500, https://doi.org/10.1016/J.RSER.2018.12.020.
[6] S. Saha, X. Zhai, S. Ehsan, S. Majeed, K. McDonald-Maier, RASA: reliability-aware scheduling approach for FPGA-based resilient embedded systems in extreme environments, IEEE Trans Syst Man Cybern Syst 52 (6) (Jun. 2022) 3885–3899, https://doi.org/10.1109/TSMC.2021.3077697.
[7] S. Esfandi, L. Rahmdel, F. Nourian, A. Sharifi, The role of urban spatial structure in energy resilience: an integrated assessment framework using a hybrid factor analysis and analytic network process model, Sustain. Cities Soc. 76 (Jan. 2022) 103458, https://doi.org/10.1016/J.SCS.2021.103458.
[8] M. Panteli, D.N. Trakas, P. Mancarella, N.D. Hatziargyriou, Power systems resilience assessment: hardening and smart operational enhancement strategies, Proc. IEEE 105 (7) (Jul. 2017) 1202–1213, https://doi.org/10.1109/JPROC.2017.2691357.
[9] B. Zhang, P. Dehghanian, M. Kezunovic, Optimal allocation of PV generation and battery storage for enhanced resilience, IEEE Trans Smart Grid 10 (1) (Jan. 2019) 535–545, https://doi.org/10.1109/TSG.2017.2747136.
[10] E. Hossain, S. Roy, N. Mohammad, N. Nawar, D.R. Dipta, Metrics and enhancement strategies for grid resilience and reliability during natural disasters, Appl. Energy 290 (May 2021) 116709, https://doi.org/10.1016/J.APENERGY.2021.116709.
[11] M. Lotfi, M. Panteli, B.V. Venkatasubramanian, M.S. Javadi, L.M. Carvalho, C. S. Gouveia, Quantifying the difference between resilience and reliability in the operation planning of mobile resources for power distribution grids, Findings (Aug. 2022), https://doi.org/10.32866/001C.37534.
[12] Q. Shi, et al., Post-extreme-event restoration using linear topological constraints and DER scheduling to enhance distribution system resilience, Int. J. Electr. Power Energy Syst. 131 (Oct. 2021) 107029, https://doi.org/10.1016/J.IJEPES.2021.107029.
[13] P. Zhang, J. Wang, W. Zhong, W. Hu, Toward governance, resilience, and economic outcomes in urban energy transition based on renewable energy allocation, Sustain. Cities Soc. 108 (Aug. 2024) 105462, https://doi.org/10.1016/J.SCS.2024.105462.
[14] M. Mahzarnia, M.P. Moghaddam, P.T. Baboli, P. Siano, A Review of the Measures to Enhance Power Systems Resilience, Institute of Electrical and Electronics Engineers Inc, Sep. 01, 2020. https://doi.org/10.1109/JSYST.2020.2965993.
[15] J.M. Home-Ortiz, O.D. Melgar-Dominguez, M.S. Javadi, J.R.S. Mantovani, J.P. S. Catalao, Improvement of the distribution systems resilience via operational resources and demand response, IEEE Trans. Ind. Appl. (2022), https://doi.org/10.1109/TIA.2022.3190241.
[16] O.A. Omitaomu, H. Niu, Artificial intelligence techniques in smart grid: a survey, Smart Cities 4 (2) (2021) 548–568, https://doi.org/10.3390/SMARTCITIES4020029.
[17] A. Esmaeel Nezhad, P.H.J. Nardelli, M.S. Javadi, S. Jowkar, T. Tavakkoli Sabour, F. Ghanavati, A hybrid optimal power flow model for transmission and distribution networks, Electr. Power Syst. Res. 245 (Aug. 2025) 111638, https://doi.org/10.1016/J.EPSR.2025.111638.
[18] M.S. Javadi, A. Esmaeel Nezhad, S. Sabramooz, Economic heat and power dispatch in modern power system harmony search algorithm versus analytical solution, Scientia Iranica 19 (6) (2012), https://doi.org/10.1016/j.scient.2012.10.033.
[19] H. Jahangirzadeh, S. Najafi Ravadanagh, N. Tagizadeghan Kalantari, Resilience-driven preventive planning of portable battery devices in the smart active distribution networks, J. Energy Storage 145 (Feb. 2026) 119830, https://doi.org/10.1016/J.EST.2025.119830.
[20] S.S. Sajjadi, A. Moghadassi, H. Rashidizadeh-Kermani, R. Kia, M. Shafie-khah, AI-driven forecasting for battery energy management in digital twin-integrated microgrids using machine learning techniques, J. Energy Storage 143 (Jan. 2026) 119556, https://doi.org/10.1016/J.EST.2025.119556.
[21] A. Roudbari, A. Nateghi, B. Yousefi-khanghah, H. Asgharpour-Alamdari, H. Zare, Resilience-oriented operation of smart grids by rescheduling of energy resources and electric vehicles management during extreme weather condition, Sustain. Energy Grids Netw 28 (Dec. 2021) 100547, https://doi.org/10.1016/J.SEGAN.2021.100547.
[22] H. Lotfi, R. Ghazi, M. bagher Naghibi-Sistani, Multi-objective dynamic distribution feeder reconfiguration along with capacitor allocation using a new hybrid evolutionary algorithm, Energy Systems 11 (3) (Aug. 2020) 779–809, https://doi.org/10.1007/s12667-019-00333-3.
[23] P. Anvari, B. Tousi, V. Talavat, M. Farhadi-Kangarlu, A smart integrated framework for resilience enhancement in distribution networks using multi-energy microgrids and distributed energy resources, Results Eng. 27 (Sep. 2025) 105635, https://doi.org/10.1016/J.RINENG.2025.105635.
[24] C.S. Bojer, Understanding machine learning-based forecasting methods: a decomposition framework and research opportunities, Int. J. Forecast. 38 (4) (Oct. 2022) 1555–1561, https://doi.org/10.1016/J.IJFORECAST.2021.11.003.
[25] S. Nourian, A. Kazemi, A two-stage optimization technique for automated distribution systems self-healing: leveraging internet data centers, power-to-hydrogen units, and energy storage systems, J. Energy Storage 85 (Apr. 2024) 111084, https://doi.org/10.1016/J.EST.2024.111084.
[26] G. Pescaroli, et al., Definitions and taxonomy for high impact low probability (HILP) and outlier events, Int. J. Disaster Risk Reduct. 127 (Sep. 2025) 105504, https://doi.org/10.1016/J.IJDRR.2025.105504.
[27] Y. Li, Q. Liu, A comprehensive review study of cyber-attacks and cyber security; emerging trends and recent developments, Energy Rep. 7 (Nov. 2021) 8176–8186, https://doi.org/10.1016/J.EGYR.2021.08.126.
[28] M. Panteli, P. Mancarella, Influence of extreme weather and climate change on the resilience of power systems: impacts and possible mitigation strategies, Electr. Power Syst. Res. 127 (Oct. 2015) 259–270, https://doi.org/10.1016/J.EPSR.2015.06.012.
[29] M. Ghanbari-Ghalehjoughi, K. Taghizad-Tavana, S. Nojavan, Resilient operation of the renewable energy and battery energy storages based smart distribution grid considering physical-cyber-attacks, J. Energy Storage 62 (Jun. 2023) 106950, https://doi.org/10.1016/J.EST.2023.106950.
[30] H. Jokar, Robust optimization for operational management of microgrids integrated with energy hubs and hydrogen refueling stations, Int. J. Hydrog. Energy 135 (Jun. 2025) 295–315, https://doi.org/10.1016/J.IJHYDENE.2025.05.006.
[31] Y. Son, H. Woo, J. Noh, P. Dehghanian, X. Zhang, S. Choi, Optimization of energy storage scheduling considering variable-type minimum SOC for enhanced disaster preparedness, J. Energy Storage 93 (Jul. 2024) 112366, https://doi.org/10.1016/J.EST.2024.112366.
[32] M.S. Javadi, C.S. Gouveia, L.M. Carvalho, A multi-temporal optimal power flow model for normal and contingent operation of microgrids, in: 2022 IEEE International Conference on Environment and Electrical Engineering and 2022 IEEE Industrial and Commercial Power Systems Europe, EEEIC / I and CPS Europe 2022, 2022, https://doi.org/10.1109/EEEIC/ICPSEUROPE54979.2022.9854741.
[33] M. Shimillas, B.V. Venkatasubramanian, N. Hatziargyriou, M. Panteli, Formation of networked microgrids for operational flexibility and resilience, in: 2024 International Conference on Smart Energy Systems and Technologies: Driving the Advances for Future Electrification, SEST 2024 - Proceedings, 2024, https://doi.org/10.1109/SEST61601.2024.10694097.
[34] A. Esmaeel Nezhad, M.S. Javadi, F. Ghanavati, T. Tavakkoli Sabour, An automated load restoration approach for improving load serving capabilities in smart urban networks, Urban Sci. 9 (7) (2025) 255, https://doi.org/10.3390/URBANSCI9070255.
[35] E.A. Javadi, M. Joorabian, H. Barati, A sustainable framework for resilience enhancement of integrated energy systems in the presence of energy storage systems and fast-acting flexible loads, J. Energy Storage 49 (May 2022) 104099, https://doi.org/10.1016/J.EST.2022.104099.

[36] A.S. Kahnamouei, S. Lotfifard, Enhancing resilience of distribution networks by coordinating microgrids and demand response programs in service restoration, IEEE Syst. J. 16 (2) (Jun. 2022) 3048–3059, https://doi.org/10.1109/JSYST.2021.3097263.

[37] M.S. Javadi, Unlocking responsive flexibility within local energy communities in the presence of grid-scale batteries, Sustain. Cities Soc. 114 (Nov. 2024) 105697, https://doi.org/10.1016/J.SCS.2024.105697.

[38] M. Panteli, C. Pickering, S. Wilkinson, R. Dawson, P. Mancarella, Power system resilience to extreme weather: fragility modeling, probabilistic impact assessment, and adaptation measures, IEEE Trans. Power Syst. 32 (5) (Sep. 2017) 3747–3757, https://doi.org/10.1109/TPWRS.2016.2641463.

[39] M. Noebels, J. Quiros-Tortos, M. Panteli, Decision-making under uncertainty on preventive actions boosting power grid resilience, IEEE Syst. J. 16 (2) (Jun. 2022) 2614–2625, https://doi.org/10.1109/JSYST.2021.3108221.

[40] M. Panteli, D.N. Trakas, P. Mancarella, N.D. Hatziargyriou, Boosting the power grid resilience to extreme weather events using defensive islanding, IEEE Trans Smart Grid 7 (6) (Nov. 2016) 2913–2922, https://doi.org/10.1109/TSG.2016.2535228.

[41] M.S. Javadi, C.S. Gouveia, L.M. Carvalho, R. Silva, Optimal power flow solution for distribution networks using quadratically constrained programming and McCormick relaxation technique, in: 2021 IEEE International Conference on Environment and Electrical Engineering and 2021 IEEE Industrial and Commercial Power Systems Europe (EEEIC / I&CPS Europe), Sep. 2021, pp. 1–6, https://doi.org/10.1109/EEEIC/ICPSEUROPE51590.2021.9584627.

[42] M. Farivar, S.H. Low, Branch flow model: relaxations and convexification-part I, IEEE Trans. Power Syst. 28 (3) (2013) 2554–2564, https://doi.org/10.1109/TPWRS.2013.2255317.

[43] M.S. Javadi, M. Lotfi, M. Gough, A.E. Nezhad, S.F. Santos, J.P.S. Catalao, Optimal spinning reserve allocation in presence of electrical storage and renewable energy sources, in: 2019 IEEE International Conference on Environment and Electrical Engineering and 2019 IEEE Industrial and Commercial Power Systems Europe (EEEIC / I&CPS Europe), Jun. 2019, pp. 1–6, https://doi.org/10.1109/EEEIC.2019.8783696.

[44] Hourly Consumption by Postal Code - 4 Digits — E-REDES, Accessed: Oct. 04, 2025. [Online]. Available: https://e-redes.opendatasoft.com/explore/dataset/consumos_horario_codigo_postal/table/?sort=datahora, Oct. 4, 2025.

[45] I.A. Quadri, S. Bhowmick, A hybrid technique for simultaneous network reconfiguration and optimal placement of distributed generation resources, Soft. Comput. 24 (15) (Aug. 2020) 11315–11336, https://doi.org/10.1007/S00500-019-04597-W/FIGURES/5.